J. Fluid Mech. (1994), *vol.* 270, *pp.* 297–330

A global stability analysis of the steady and periodic cylinder wake

By BERND R. NOACK AND HELMUT ECKELMANN
Max-Planck-Institut für Strömungsforschung, Bunsenstraße 10, D-37 073 Göttingen, Germany

(Received 17 March 1993 and in revised form 23 September 1993)

A global, three-dimensional stability analysis of the steady and the periodic cylinder wake is carried out employing a low-dimensional Galerkin method. The steady flow is found to be asymptotically stable with respect to all perturbations for $Re < 54$. The onset of periodicity is confirmed to be a supercritical Hopf bifurcation which can be modelled by the Landau equations. The periodic solution is observed to be only neutrally stable for $54 < Re < 170$. While two-dimensional perturbations of the vortex street rapidly decay, three-dimensional perturbations with long spanwise wavelengths neither grow nor decay. The periodic solution becomes unstable at $Re = 170$ by a perturbation with the spanwise wavelength of 1.8 diameters. This instability is shown to be a supercritical Hopf bifurcation in the spanwise coordinate and leads to a three-dimensional periodic flow. Finally the transition scenario for higher Reynolds numbers is discussed.

1. Introduction

The flow around a circular cylinder can be considered as a prototype of the bluff-body wakes because of the simplicity of the boundary conditions and the complexity of the physical processes involved. In fact many physical mechanisms of viscous incompressible fluid motion can be studied in this flow, e.g. potential flow, laminar and turbulent boundary layers, separation, shear-layer and vortex dynamics, a near-wake which is dominated by nonlinear phenomena, and a far-wake which is governed by linear convection and dissipation processes. This complexity makes the cylinder wake a rewarding object of study for the experimentalist and a challenge for the theoretician.

Because of the intensive research which the cylinder wake has enjoyed for over a hundred years, there exists little controversy about the main properties of the post-transient flow. These properties depend on the Reynolds number $Re = UD/\nu$, where U, D, and ν represent the oncoming velocity, the cylinder diameter, and the kinematic viscosity of the fluid, respectively. For $Re < 5$, the steady velocity field has only one separation point. In the range $5 < Re < 50$, a steady vortex pair at the rear of the cylinder grows with Re. For $50 < Re < 175$, two-dimensional periodic vortex shedding is observed. This vortex shedding is superimposed by three-dimensional fluctuations for higher Reynolds numbers. These critical Reynolds numbers for the onset of periodicity and three-dimensionality depend on the authors and vary in a small range.

In contrast to the asymptotic behaviour, little is known about the transients and the stability properties of cylinder wake. For instance, is the onset of periodicity at the critical Reynolds number $Re_{crit} \approx 50$ typically a two-dimensional process or do infinitesimal three-dimensional perturbations lead via highly three-dimensional transients to the periodic solution?

Numerical simulations (see, for instance, Patel 1978) indicate that the two-

dimensional period wake is stable with respect to two-dimensional perturbations for Reynolds numbers up to 500. Karniadakis & Triantafyllou's (1992) pioneering three-dimensional simulations yield that the wake is also globally stable with respect to three-dimensional perturbations which have spanwise wavelengths of π and $\frac{1}{2}\pi$ diameters for $Re < 175$. Yet it is striking that in most experimental investigations the vortices do not shed parallel to the cylinder axis – even with aspect ratios far in excess of a hundred. Instead, a variety of different three-dimensional vortex formations is observed (Williamson 1989; König, Eisenlohr & Eckelmann 1990, 1992; Hammache & Gharib 1991). Parallel shedding is only achieved with carefully selected end conditions at the cylinder. Do the experimental observations imply that the currently available wind-tunnel facilities are too inaccurate for a realization of the stable two-dimensional periodic flow or are there some non-decaying three-dimensional processes involved?

Another discrepancy between experimental and numerical works relates to the onset of three-dimensionality at the second critical Reynolds number $Re_{crit,2} \approx 175$. Williamson (1988*a*, *b*) reports a hysteretic hard transition from two-dimensional vortex shedding to an irregular three-dimensional wake. In contrast Karniadakis & Triantafyllou (1992) observe a soft transition to a periodic three-dimensional shedding.

Naturally, a global three-dimensional stability analyses of the steady and the periodic flow is the most suitable forum to elucidate these problems. At present, only two-dimensional analyses of the stationary problem seem to exist, by Zebib (1987), Jackson (1987), and other groups. These stability analyses are based on finite-difference and finite-element techniques with of the order of 10000 grid points. They cannot easily be generalized to three-dimensional perturbations. For a discretization of the three-dimensional cylinder wake of the order of 1000000 grid points are needed. Such high-dimensional eigenvalue problems can hardly be handled with presently available algorithms. These numerical problems apply even more to the Floquet stability analysis of the periodic flow.

Local stability investigations of the cylinder wake (see, for instance, the review articles of Oertel 1990 and Huerre & Monkewitz 1990) have contributed much to the understanding of two-dimensional vortex shedding. These methods may also elucidate partial three-dimensional aspects of vortex shedding (e.g. Triantafyllou 1990). Yet they cannot provide insights into the global properties of the most dangerous perturbations and rest on simplifying assumptions of the flow.

In order to carry out the global stability analyses, the authors have constructed a low-dimensional Galerkin method (Noack 1992; Noack & Eckelmann 1993, 1994*a*). Section 2 provides a brief description of the Galerkin method employed and outlines the numerical techniques for the linear stability analysis of the steady and periodic flow. In §§3 and 4 results of the stability investigations of the steady and periodic solutions are presented. In both sections the evolution of finite perturbations in the framework of the fully nonlinear Navier–Stokes equations are also investigated. In §5 phenomenological models for the observed instability processes are developed. Section 6 summarizes and discusses the results presented.

2. Numerical methods

In this section the numerical methods employed for the investigations that follow are discussed. First (§2.1) the Galerkin method for the computation of the three-dimensional flow is briefly outlined. In §§2.2 and 2.3 the algorithms for the stability analysis of the steady solution and for the Floquet analysis of the periodic flow are described, respectively.

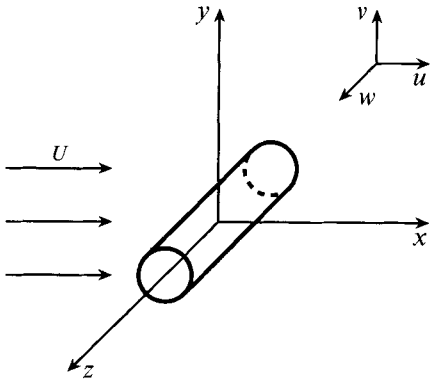

FIGURE 1. Coordinate system.

2.1. *Galerkin method*

The present Galerkin method generalizes the two-dimensional technique of Noack & Eckelmann (1991, 1992) to three dimensions employing Zebib's (1987) ansatz for the incompressible flow.

The flow is described in a Cartesian coordinate system x, y, z (see figure 1). These coordinates are summarized in a position vector $\boldsymbol{x} = (x, y, z)$. The unit-vectors in the x-, y-, and z-directions are denoted by $\hat{\boldsymbol{e}}_x$, $\hat{\boldsymbol{e}}_y$, and $\hat{\boldsymbol{e}}_z$, respectively. The x-axis is aligned with the oncoming velocity $U\hat{\boldsymbol{e}}_x$ and the z-axis coincides with the axis of the circular cylinder, the y-axis being perpendicular to both. The x-, y-, and z-components of the velocity vector $\boldsymbol{u}$ are u, v, and w. Alternatively, a cylindrical coordinate system r, ϕ, z is used where $r = (x^2+y^2)^{\frac{1}{2}}$, $\phi = \arctan(y/x)$, and z coincides with the Cartesian coordinate. The time is denoted by t. In the following all physical quantities are assumed to be normalized with the cylinder radius R and the velocity U.

According to Zebib (1987) the incompressible velocity field around a circular cylinder can be expressed in terms of two generalized stream functions Ψ and Φ via

$$\boldsymbol{u} = \boldsymbol{\nabla} \times \{\Psi \hat{\boldsymbol{e}}_z\} + \boldsymbol{\nabla} \times \boldsymbol{\nabla} \times \{\Phi \hat{\boldsymbol{e}}_z\}, \tag{1}$$

where $\boldsymbol{\nabla}\times$ represents the curl operator. A similar ansatz is used by Busse (1991) and Clever & Busse (1990) for the Rayleigh–Bénard problem and for the Taylor–Couette flow.

The boundary conditions at the cylinder and at infinity are fulfilled by using Zebib's (1987) equations (7*a*) and (7*b*), which read

$$\Psi = \frac{\partial}{\partial r}\Psi = \Phi = \frac{\partial}{\partial r}\Phi = \frac{\partial^2}{\partial r^2}\Phi = 0 \quad \text{at} \quad r = 1, \tag{2}$$

$$\Psi \to r\sin\phi \quad \text{and} \quad \Phi \to 0 \quad \text{for} \quad r \to \infty. \tag{3}$$

In addition, we assume a spanwise periodicity with wavelength L and wavenumber $k_z = 2\pi/L$ as in the numerical simulations of Karniadakis & Triantafyllou (1992) and Tomboulides, Triantafyllou & Karniadakis (1992), i.e.

$$\Psi(r, \phi, z) = \Psi(r, \phi, z+L) \quad \text{and} \quad \Phi(r, \phi, z) = \Phi(r, \phi, z+L). \tag{4}$$

For the evolution equation of the generalized stream functions, the Laplace operators in two and three dimensions,

$$\Delta_{r,\phi} = \frac{\partial^2}{\partial r^2} + \frac{1}{r}\frac{\partial}{\partial r} + \frac{1}{r^2}\frac{\partial^2}{\partial \phi^2} \quad \text{and} \quad \Delta = \Delta_{r,\phi} + \frac{\partial^2}{\partial z^2}$$

are introduced. The Navier–Stokes equations can now be easily expressed as coupled partial differential equations for Ψ and Φ (see Zebib's equations (6*a*) and (6*b*)):

$$\frac{\partial}{\partial t}\Delta_{r,\phi}\Psi = \frac{2}{Re}\Delta\Delta_{r,\phi}\Psi - \hat{\boldsymbol{e}}_z\cdot\boldsymbol{\nabla}\times(\boldsymbol{u}\times\{\boldsymbol{\nabla}\times\boldsymbol{u}\}), \tag{5}$$

$$\frac{\partial}{\partial t}\Delta\Delta_{r,\phi}\Phi = \frac{2}{Re}\Delta^2\Delta_{r,\phi}\Phi - \hat{\boldsymbol{e}}_z\cdot\boldsymbol{\nabla}\times\boldsymbol{\nabla}\times(\boldsymbol{u}\times\{\boldsymbol{\nabla}\times\boldsymbol{u}\}), \tag{6}$$

where $\boldsymbol{u}$ is given by (1). It should be noted that Zebib's velocity field ansatz and his evolution equations generalize the two-dimensional stream-function formalism by one additional function Φ, which vanishes for a two-dimensional flow.

A straightforward three-dimensional generalization of Zebib's (1987) two-dimensional Galerkin method yields for the lowest spanwise resolution more than 10000 modes.† With such a high-dimensional system, a stability analysis is hardly possible with the currently available computer power. Hence, we have generalized the low-dimensional Galerkin method of Noack & Eckelmann (1991, 1992) for the two-dimensional cylinder wake to three dimensions. In the two-dimensional method, the *basic mode* is defined by

$$\Psi^{(0)} = (r-1/r)\left[1-\exp\left(-\frac{r-1}{\delta_{bm}}\right)\right]\sin\phi, \tag{7}$$

with $\delta_{bm} = 4/Re^{\frac{1}{2}}$. This mode satisfies the no-slip conditions at the cylinder and approaches the potential solution at infinity. Equations (2)–(4) then imply that the new functions

$$\Psi^{(1)} = \Psi - \Psi^{(0)} \quad \text{and} \quad \Psi^{(2)} = \Phi \tag{8}$$

fulfil homogeneous boundary conditions at the cylinder

$$\Psi^{(\kappa)} = \ldots = \frac{\partial^\kappa}{\partial r^\kappa}\Psi^{(\kappa)} = 0 \quad \text{for} \quad \kappa = 1,2, \tag{9}$$

at infinity

$$\Psi^{(\kappa)} \to 0 \quad \text{for} \quad \kappa = 1,2, \tag{10}$$

and in the spanwise direction

$$\Psi^{(\kappa)}(r,\phi,z) = \Psi^{(\kappa)}(r,\phi,z+L) \quad \text{for} \quad \kappa = 1,2. \tag{11}$$

The functions $\Psi^{(\kappa)}$ can be approximated by Fourier expansions with *expansion modes*. These modes are based on the two function systems $\{R_i^{(\kappa)}(r)\}_{i=0}^{\infty}$ ($\kappa = 1,2$) for the radial coordinate and two κ-independent systems $\{\Phi_j(\phi)\}_{j=-\infty}^{\infty}$ and $\{Z_k(z)\}_{k=-\infty}^{\infty}$ for the azimuthal and spanwise coordinates. These function systems result from mathematical and physical considerations outlined by Noack (1992) and Noack & Eckelmann (1994*a*) and are defined in Appendix A. It should be noted that the construction of the radial and azimuthal function systems differs from Zebib's choice. The resulting $\mathscr{H}_{I,J,K}$ *Galerkin approximation* for $\Psi^{(\kappa)}$ reads, in the Einstein summation convention,

$$\Psi^{(\kappa)}(r,\phi,z,t) = a_{ijk}^{(\kappa)}(t)\, R_i^{(\kappa)}(r)\, \Phi_j(\phi)\, Z_k(z) \quad \text{for} \quad \kappa = 1,2, \tag{12}$$

where the $a_{ijk}^{(\kappa)}$ denote the time-dependent Fourier coefficients and

$$\Psi_{ijk}^{(\kappa)} = R_i^{(\kappa)}(r)\, \Phi_j(\phi)\, Z_k(z)$$

the expansion modes. The indices i,j,k are summed over the index sets $\mathscr{I} = \{0,1,\ldots,I\}$, $\mathscr{J} = \{-J,\ldots,0,\ldots,J\}$, and $\mathscr{K} = \{-K,\ldots,0,\ldots,K\}$. This approximation exactly fulfils the boundary conditions (9)–(11) for all choices of the Fourier coefficients and can

† This number of modes is estimated assuming two expansions for Ψ and $\Phi \times 23$ radial modes ($N_r = 22$) $\times$ 89 azimuthal modes ($N_\theta = 44$) $\times$ 3 spanwise modes. The index bounds $N_r = 22$ and $N_\theta = 44$ are also used in Zebib's (1987) stability analysis.

naturally resolve the velocity field with arbitrary precision for sufficiently large index bounds I, J, and K.

For the present stability investigations, the $\mathscr{H}_{6,4,1}$ approximation is chosen. This choice guarantees a sufficiently accurate numerical simulation of the two- and three-dimensional flows at moderate Reynolds numbers. On the other hand, the CPU times for global three-dimensional stability analyses of the steady and periodic solutions on a SPARCstation2 remain still reasonable.

The equation of motion for the Fourier coefficients is derived from Zebib's (1987) evolution equations (5) and (6) in a canonical *Galerkin projection* as follows. First, the Galerkin approximations (8) and (12) are substituted in Zebib's equations. Equations (5) and (6) are multiplied with the Hilbert-space weight function $w = r^{-\frac{3}{2}}$ and the projection modes $\Psi_{ijk}^{(\kappa)}$ for $\kappa = 1$ and 2, respectively. The resulting terms are then integrated over the domain of the velocity field $\Omega = \{(r, \phi, z): r \geqslant 1 \text{ and } 0 \leqslant z \leqslant L\}$. Taking the indices of the projection modes from the same set as for the Galerkin approximation, we have as many equations as unknown Fourier coefficients. The resulting system of autonomous first-order differential equations can be solved for the temporal derivatives of the Fourier coefficients, thus yielding a system of the form

$$\frac{\mathrm{d}}{\mathrm{d}t} a_{ijk}^{(\kappa)} = c_{ijk}^{(\kappa)} + \sum_{\mu=1}^{2} l_{ijk;lmn}^{(\kappa;\mu)} a_{lmn}^{(\mu)} + \sum_{\mu=1}^{2} \sum_{\nu=1}^{2} q_{ijk;lmn,pqs}^{(\kappa;\mu,\nu)} a_{lmn}^{(\mu)} a_{pqs}^{(\nu)} \tag{13}$$

for $\kappa = 1, 2$, where the coefficients $c_{ijk}^{(\kappa)}$, $l_{ijk;lmn}^{(\kappa;\mu)}$, $q_{ijk;lmn,pqs}^{(\kappa;\mu,\nu)}$ of the constant, linear, and quadratic terms represent volume integrals over products of the projection and derivatives of the expansion modes. In this and all following equations the Einstein summation convention for the subscript is employed. Details about the Galerkin projection and the numerical realization of the autonomous system can be obtained from Noack (1992) and Noack & Eckelmann (1994*a*).

The above equations and the modes, which are specified in Appendix A, uniquely define the $\mathscr{H}_{I,J,K}$ Galerkin method. For $K = 1$, (13) has two invariant subspaces: the subspace $\mathscr{H}_{I,J,1}^{(+)}$ spanned by all Fourier coefficients with $k \leqslant 0$ for $\kappa = 1$ and $k > 0$ for $\kappa = 2$ and $\mathscr{H}_{I,J,1}^{(-)}$ with the restriction $k \geqslant 0$ for $\kappa = 1$ and $k < 0$ for $\kappa = 2$. From the definition of Z_k in Appendix A, it can be inferred that the subsets of expansion modes in both subspaces are simply related by a substitution of $\sin(k_z z)$ with $\cos(k_z z)$ and vice versa. Both reduced Galerkin methods contain all two-dimensional solutions and have the same stability and Floquet spectra. The corresponding eigenmodes and Floquet modes of the $\mathscr{H}_{I,J,1}^{(+)}$ and $\mathscr{H}_{I,J,1}^{(-)}$ system are related by simple symmetry transformations. Furthermore, both systems are numerically observed to contain the most dangerous part of the full $\mathscr{H}_{I,J,1}$ stability and Floquet spectra for the Reynolds numbers and wavenumbers considered. Therefore, we restrict the 378-dimensional $\mathscr{H}_{6,4,1}$ Galerkin method chosen to the 189-dimensional $\mathscr{H}_{6,4,1}^{(+)}$ subspace, in the following investigations. This simplification has no impact on the dangerous eigen- and Floquet modes analysed but allows for carrying out the stability investigations on a small workstation. The results obtained with the $\mathscr{H}_{6,4,1}^{(+)}$ method have been validated with other resolutions, namely with $\mathscr{H}_{4,2,1}^{(+)}$, $\mathscr{H}_{4,4,1}^{(+)}$, and $\mathscr{H}_{6,6,1}^{(+)}$ approximations.

For the numerical methods of the stability investigations, the quadrupol index (κ, i, j, k) in the autonomous system (13) is inconvenient. Mapping this index bijectively on a single index $\Pi(\kappa, i, j, k) \in \{1, 2, \ldots, N\}$, where N is the number of modes, (13) can be rewritten in the simpler form

$$\frac{\mathrm{d}}{\mathrm{d}t} a_i = f_i(a_1, \ldots, a_N) = c_i + l_{i;j} a_j + q_{i;j,k} a_j a_k. \tag{14}$$

The Fourier coefficients and the coefficients for the constant, linear, and quadratic terms are given by $a_{\Pi(\kappa,i,j,k)} = a^{(\kappa)}_{ijk}$, $c_{\Pi(\kappa,i,j,k)} = c^{(\kappa)}_{ijk}$, $l_{\Pi(\kappa,i,j,k));\Pi(\mu,l,m,n)} = l^{(\kappa;\mu)}_{ijk;lmn}$, and $q_{\Pi(\kappa,i,j,k);\Pi(\mu,l,m,n),\Pi(\nu,p,q,s)} = q^{(\kappa;\mu,\nu)}_{ijk;lmn,pqs}$, respectively. In the following, bold-face symbols without indices denote the corresponding N-dimensional vector of all components, for example the mode vector $\boldsymbol{a} = (a_1, \ldots, a_N)$ and the flow $\boldsymbol{f} = (f_1, \ldots, f_N)$.

2.2. *Stability analysis of the steady flow*

The stability analysis of the steady flow consists of three steps.

In the first step, the (possibly unstable) steady solution $a^{(s)}_i$ of (14) is computed. Fortunately, this fixed point is globally asymptotically stable on the invariant subspace which is spanned by the two-dimensional antisymmetrical modes for all Reynolds numbers considered. This subspace is spanned by all Fourier coefficients $a^{(1)}_{i,j,0}$ with $j > 0$; the other coefficients vanish identically. If the initial condition for (14) lies in this subspace, the numerical integration will always converge to the fixed point, which represents the two-dimensional steady flow. Convergence is typically achieved within 100 time units (R/U), starting from the origin of the mode space, and is checked by requiring that the right-hand side of (14) practically vanishes, i.e. is less than 10^{-4}.

In the second step, the *stability matrix* is calculated. This matrix $\boldsymbol{S} = (l^*_{i;j})_{i=1,\ldots,N;\ j=1,\ldots,N}$, represents the Jacobian of the flow $\boldsymbol{f}$ at the fixed point $\boldsymbol{a}^{(s)}$. Its elements are given by

$$l^*_{i;j} = l_{i;j} + (q_{i;j,k} + q_{i;k,j})\, a^{(s)}_k. \tag{15}$$

With this matrix, the evolution equation for the deviation of the steady solution $\boldsymbol{a}^* = \boldsymbol{a} - \boldsymbol{a}^{(s)}$ reads

$$\frac{\mathrm{d}}{\mathrm{d}t} a^*_i = f^*_i(a_1, \ldots, a_N) = l^*_{i;j}\, a^*_j + q_{i;j,k}\, a^*_j\, a^*_k. \tag{16}$$

In the final step, the eigenvalues λ_l of the stability matrix are computed, using the subroutines BALANC, ELMHES, and HQR from Press *et al.* (1986), in this order. The accuracy of the numerically obtained λ_l is of the order of 10^{-4} and is checked for each spectrum. The eigenvalues are generally complex and expressed in the form $\lambda_l = \pi(\sigma_l + \mathrm{i}St_l)$, where σ_l denotes the growth rate and the St_l the Strouhal number, except for the sign. The eigenvalues are assumed to be ordered with respect to their growth rates, i.e. $\sigma_1 \geqslant \sigma_2 \geqslant \ldots$. The corresponding eigenvectors $\boldsymbol{a}^{(s),l}$ are calculated with the inverse iteration method and are normalized to yield an Euclidean norm of unity. Without loss of generality the eigenvector of a real eigenvalue can be considered to be real. In this case the normalized eigenvector is indeterminate by a factor ± 1. The temporal evolution with respect to the linearized autonomous system is given by $\boldsymbol{a}^{(s),l} \mathrm{e}^{\sigma_l t}$. In contrast, the normalized eigenvectors of a complex eigenvalue are generally complex and indeterminate by a complex factor of unit modulus, which can be interpreted as a phase shift for one revolution. In the stability analysis, we consider only the real part of the time-dependent solution $\boldsymbol{a}^{(s),l} \mathrm{e}^{\sigma_l + \mathrm{i}St_l t}$ of the linearized system. Obviously, if all growth rates σ_l are negative, all perturbations decay and the steady solution is linearly stable. If there exists one eigenvalue with a positive σ_l, 'almost all' perturbations will generally grow and the steady solution is unstable. It should be noted that the eigenvectors and solutions of the linearized system, called *eigenmodes* in the following, correspond to velocity fields in the physical space via equations (1), (7), (8), (12), and the index map Π.

We distinguish between *two-dimensional eigenvalues* corresponding to two-dimensional eigenvectors and *three-dimensional* ones of eigenvectors which represent three-dimensional velocity fields. The first are denoted by $\lambda^{(2D)}_l = \pi(\sigma^{(2D)}_l + \mathrm{i}St^{(2D)}_l)$, while

the latter eigenvalues have a (3*D*) superscript. Both groups are assumed to be ordered with respect to the grow rates, i.e. $\sigma_1^{(2D)} \geqslant \sigma_2^{(2D)} \geqslant \ldots$ and $\sigma_1^{(3D)} \geqslant \sigma_2^{(3D)} \geqslant \ldots$.

2.3. *Floquet analysis of the periodic flow*

The stability analysis of the periodic flow (the *Floquet analysis*) is carried out in three steps for a given Reynolds number and a fixed spanwise wavelength.

First, the periodic solution $\boldsymbol{a}^{(p)}(t)$ of (14) is numerically computed. For all Reynolds numbers considered, the *two-dimensional* periodic solution is asymptotically stable in an invariant 63-dimensional subspace which is spanned by the two-dimensional modes $a_{i,j,0}^{(1)}$. Hence, sufficiently long transients finally converge to the (possibly unstable) periodic solution. Convergence is typically achieved in 100 to 200 time units. In contrast, the three-dimensional periodic solution does not lie in a linear subspace and can hence only be computed if it is stable.

In the second step, the *Floquet matrix* is calculated. For this purpose, the fundamental solution of the first variational form

$$\frac{\mathrm{d}}{\mathrm{d}t}\boldsymbol{a}' = \left.\frac{\partial \boldsymbol{f}}{\partial \boldsymbol{a}}\right|_{\boldsymbol{a}^{(p)}} \cdot \boldsymbol{a}' \tag{17}$$

for the infinitesimal perturbation $\boldsymbol{a}'$ on the T-periodic solution $\boldsymbol{a}^{(p)}$ is numerically computed. In (17), $\partial \boldsymbol{f}/\partial \boldsymbol{a}|_{\boldsymbol{a}^{(p)}}$ represents the T-periodic Jacobian matrix of $\boldsymbol{f}$ evaluated at $\boldsymbol{a}^{(p)}$. The solutions of (17) can be symbolically expressed by the map $\Phi_t: \mathscr{R}^N \mapsto \mathscr{R}^N$ with $\boldsymbol{a}(t) = \Phi_t(\boldsymbol{a}(0))$. With this map, the canonical choice for the fundamental system is given by $t \mapsto \{\Phi_t(\hat{\boldsymbol{e}}_m)\}_{n=1}^N$, $\hat{\boldsymbol{e}}_m$ being the mth unit vector in the mode space $\mathscr{R}^N$.

Finally, the eigenvalues μ_m and the corresponding eigenvectors $\boldsymbol{a}^{(p),m}$ are computed from the $N \times N$ Floquet matrix $\boldsymbol{F}$ with the columns $\Phi_T(\hat{\boldsymbol{e}}_m)$ for $m = 1, 2, \ldots, N$. The same numerical algorithms as in the stability analysis of the steady solutions are employed. The eigenvalues μ_m are called *Floquet multipliers* and the corresponding *Floquet modes* $\boldsymbol{a}^{(p)/m}(t) := \Phi_t(\boldsymbol{a}^{(p),m})$ satisfy $\boldsymbol{a}^{(p)/m}(T) = \mu_m \boldsymbol{a}^{(p)/m}(0)$ by construction (see Jordan & Smith 1988, §9.2). Under generic conditions, every solution of (17) can be expressed by $\boldsymbol{a}'(t) = \sum_{m=1}^N \alpha_m \boldsymbol{a}^{(p)/m}(t)$ with time-independent coefficients α_m. The contribution $\alpha_m \boldsymbol{a}^{(p)/m}(t)$ vanishes as $t \to \infty$ if $|\mu_m| < 1$ or explodes if $|\mu_m| > 1$. Therefore, the Floquet multipliers are assumed to be ordered with respect to their moduli $|\mu_1| \leqslant |\mu_2| \leqslant \ldots$. For periodic motion, there always exists a $+1$ multiplier which corresponds to a phase shift on the limit cycle. This contribution is neglected in what follows, since this mode is immaterial for the Poincaré stability properties of the limit cycle. It is important to note that the Floquet modes are derived for the mode space but can also be defined in the physical space.

In analogy to the eigenvalues of the stationary stability problem, we distinguish between two- and three-dimensional Floquet multipliers which are denoted by $\mu^{(2D)} = \mu_{r,l}^{(2D)} + \mathrm{i}\mu_{i,l}^{(2D)}$ and $\mu^{(3D)} = \mu_{r,l}^{(3D)} + \mathrm{i}\mu_{i,l}^{(3D)}$, respectively. Both groups are ordered with respect to the moduli in the same manner as the whole Floquet spectrum $\{\mu_l\}_{l=1,\ldots,N}$.

3. Stability of the steady flow

In §§3.1 and 3.2 the stability of the steady flow around a circular cylinder with respect to two-dimensional and three-dimensional infinitesimal disturbances is investigated. Finally, the evolution of finite disturbances is described in §3.3.

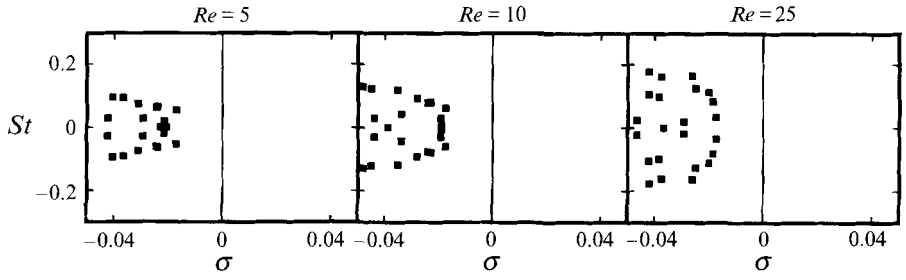

FIGURE 2. Two-dimensional stability spectra of the steady solution for $Re = 5$, 10, and 25. Each solid square represents one eigenvalue $\lambda_i^{(2D)} = \pi(\sigma_i^{(2D)} + \mathrm{i}St_i^{(2D)})$.

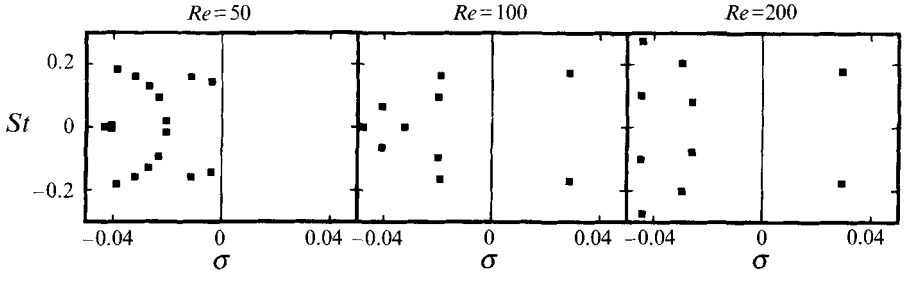

FIGURE 3. Same as figure 2 but for $Re = 50$, 100, and 200.

3.1. *Two-dimensional stability analysis*

The steady flow around a circular cylinder has been subject to a variety of global, two-dimensional stability analyses (e.g. Jackson 1987; Zebib 1987; Morzyński & Thiele 1991). These investigations yield the most dangerous eigenvalue pair $\lambda_{1,2} = \pi(\sigma_1 \pm \mathrm{i}St_1)$ with the corresponding eigenmode and are based on accurate finite-difference or finite-element methods with approximately 10000 grid points. The present Galerkin method with only 63 two-dimensional expansion modes allows for the first time some insight into the most dangerous part of the stability spectrum and higher-order eigenmodes to $\lambda_n, n > 1$. This insight and the low computational costs are paid for by a slight loss of the accuracy of $\lambda_{1,2}$ as compared to grid-based stability analyses.

Figure 2 displays the spectra of the stable steady flow at low Reynolds numbers. The most pronounced characteristics of the spectra are the nearly parabola-shaped boundary, the parabola becoming narrower towards the real axis with decreasing Reynolds number. This behaviour of the spectrum is typical for convection–dissipation systems, $1/Re$ being considered as the viscosity (see Appendix B).

It should be noted that the spectra for low Reynolds numbers do not contain a pronounced complex-conjugated eigenvalue pair $\lambda_{1,2} = \pi(\sigma_1 \pm \mathrm{i}St_1)$, which would define a characteristic frequency for the decaying disturbances. This feature explains Sreenivasan, Strykowski & Olinger's (1991) experimental observation that the von Kármán vortex street cannot be excited by periodical perturbations for $Re < 25$, even with very large amplitudes. Such an eigenvalue pair leaves the 'cloud' of the other eigenvalues only for Reynolds numbers somewhat above 30. These eigenvalue migrations lead to mode jumps which had already been discovered by Zebib (1987).

Figure 3 displays the stability spectra for the Reynolds numbers $Re = 50$, 100, and 200, i.e. when the asymptotic solution is steady, periodic, and non-periodic, respectively. With increasing Re, a single complex-conjugated eigenvalue pair moves to

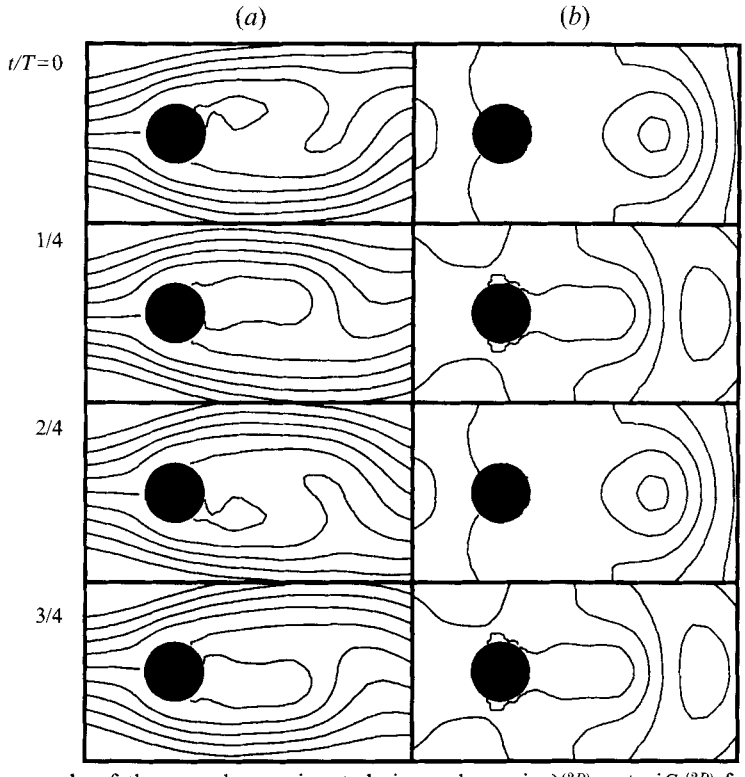

FIGURE 4. Eigenmode of the complex-conjugated eigenvalue pair $\lambda_{1,2}^{(2D)} = \pm \pi i St_1^{(2D)}$ for $Re = Re_{crit}$. Column (*b*) illustrates the streamlines in the (x, y)-plane of the eigenmode for the instants $t/T = 0$, $\frac{1}{4}$, $\frac{2}{4}$, $\frac{3}{4}$ from top to bottom, where $T = 2/St_1^{(2D)}$ is the period. This eigenmode has been multiplied by the arbitrary factor 3.5 after the normalization to yield reasonable velocity amplitudes. Column (*a*) displays the streamlines of the eigenmode superimposed on the steady flow at the same instants. In both columns the streamlines represent Ψ-values which are integral multiples of 0.5.

the right, crossing the imaginary axis at $Re_{crit} = 54$ with the Strouhal number value $St_{crit} = 0.149$, and remains the only contribution to the $\sigma > 0$ half-plane. It should be noted that the discreteness of the spectrum including the non-degenerate, isolated eigenvalue pair $\lambda_{1,2}$ is not a numerical discretization effect but can be derived from mathematical separability arguments (see Noack & Eckelmann 1992).

The crossing of the (isolated non-degenerate) eigenvalue pair with $\sigma = 0$ represents a Hopf bifurcation and marks the onset of periodicity in the cylinder wake. The present values of Re_{crit}, St_{crit} of this bifurcation significantly exceed the numerically obtained values of Zebib (1987) of $Re_{crit} = 45$, $St_{crit} = 0.11$–0.13, and of Jackson (1987) of $Re_{crit} = 46.184$, $St_{crit} = 0.13804$, and the experimentally determined values of Provansal, Mathis & Boyer (1987) of $Re_{crit} = 47$, $St_{crit} = 0.12$ (Roshko frequency). The delayed onset of vortex shedding and the too-large frequency result from an insufficient far-wake resolution of the present Galerkin approximation and are explained in Noack & Eckelmann (1994*a*). As expected, the Galerkin method yields significantly better values with more expansion modes, e.g. $Re_{crit} = 50$ and $St_{crit} = 0.132$ for 117 modes ($I = 8$, $J = 6$). Yet increasing the number of modes does not affect the qualitative conclusions drawn from the stability investigations. Hence, the Galerkin approximation defined in §2.1 suffices. A detailed convergence analysis of Re_{crit}, St_{crit}, and other quantities for index bounds I, J up to 10 was carried out by Noack & Eckelmann (1994*a*).

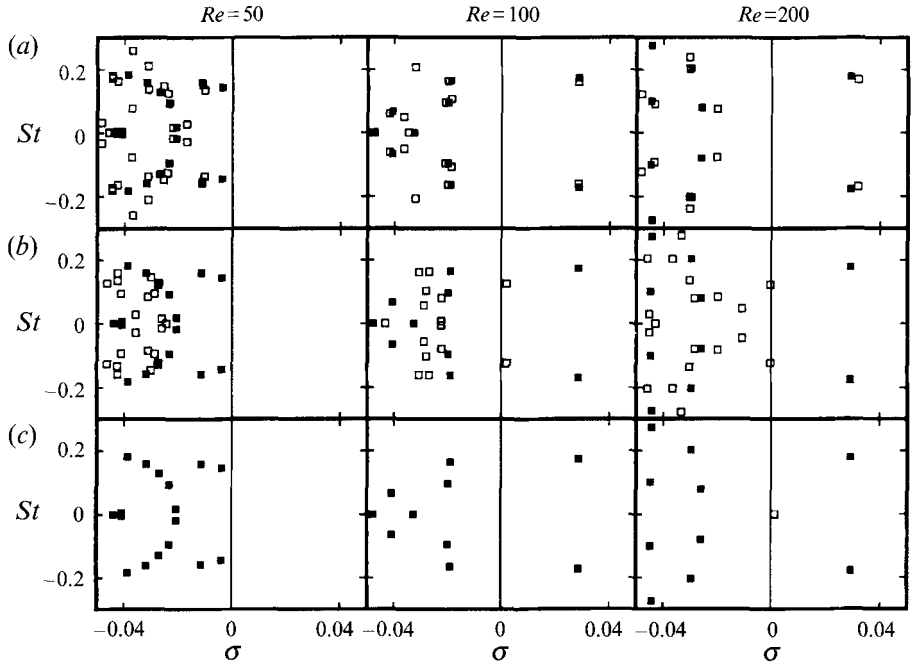

FIGURE 5. Stability spectra of the steady solution for $Re = 50$, 100, and 200 and for (*a*) $k_z = 0.5$, (*b*) 1, and (*c*) 2. The solid squares represents k_z-independent, two-dimensional eigenvalues $\lambda_l^{(2D)} = \pi(\sigma_l^{(2D)} + \mathrm{i}St_l^{(2D)})$, while the open ones refer to three-dimensional eigenvalues $\lambda_l^{(3D)} = \pi(\sigma_l^{(3D)} + \mathrm{i}St_l^{(3D)})$.

The eigenmode of $\lambda_{1,2} = \pm\pi St_1$ at $Re = Re_{crit}$ is illustrated in figure 4 (column *b*). The originally normalized eigenmode has been multiplied by an arbitrary factor of 3.5 in order to yield velocity amplitudes which are typical for the von Kármán vortex street. The streamlines of the eigenmode indicate a row of extended vortices with alternating sign on the positive x-axis convecting downstream. Superimposing this eigenmode on the steady flow yields a velocity field which is similar to the vortex street behind a circular cylinder at higher Reynolds numbers (see column *a* of figure 4). These results confirm Jackson's (1987) and Morzyński & Thiele's (1991) stability investigations with high-dimensional grid methods and show that the low-dimensional Galerkin method correctly describes the physical processes of the cylinder wake.

3.2. *Three-dimensional stability analysis*

The low-dimensional Galerkin method allows for the first time a global, *three-dimensional* stability analysis of the steady cylinder wake. Figure 5 shows the spectra for the Reynolds numbers $Re = 50$, 100, 200 and for the wavenumbers $k_z = 0.5$, 1, 2. For somewhat larger wavenumbers than 2 and for low Reynolds numbers, say below 30, the three-dimensional disturbances have small (negative) growth rates and are dissipated much more rapidly than their most dangerous two-dimensional counterparts. The spectra (figure 5) show two groups of dangerous three-dimensional eigenvalues (i.e. $\lambda_l^{(3D)} = \pi(\sigma_l^{(3D)} + \mathrm{i}St_l)$ with $\sigma_l^{(3D)} > 0$) in addition to the two-dimensional eigenvalues. The first group (see second and third columns of figure 5*a*, *b*) is a complex-conjugated pair $\lambda_{1,2}^{(3D)} = \pi(\sigma_1^{(3D)} \pm \mathrm{i}St_1^{(3D)})$ which crosses the $\sigma = 0$ axis for $k_z \approx 1$ and for sufficiently large Re-values. This pair converges to $\lambda_{1,2}^{(2D)} = \pi(\sigma_1^{(2D)} \pm \mathrm{i}St_1^{(2D)})$ in the limit $k_z \to 0$. It should be noted that $St_1^{(3D)}$ remains smaller than $St_1^{(2D)}$ for all Reynolds

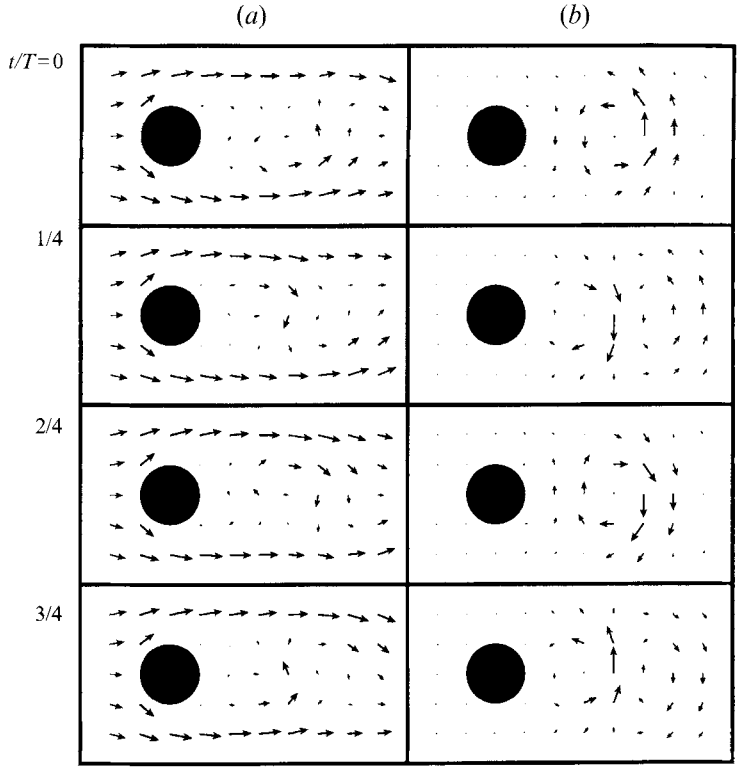

FIGURE 6. Eigenmode of the complex-conjugated eigenvalue pair $\lambda_{1,2}^{(3D)} = \pi(0.0285 \pm i0.161)$ for $Re = 100$ and $k_z = 0.5$. Column (*b*) illustrates the velocity field of the eigenmode in the $z = 0$ plane for the instants $t/T = 0, \frac{1}{4}, \frac{2}{4}$, and $\frac{3}{4}$. This eigenmode has been multiplied by the arbitrary factor 2 after the normalization. In column (*a*) the steady solution is added to this mode. The arrows are parallel to the tangential velocity component $(u, v, 0)$ in the $z = 0$ plane; their length is half the magnitude of this velocity component, i.e. $0.5(u^2+v^2)^{\frac{1}{2}}$ in the column (*a*) and twice as much in column (*b*). This implies that an arrow whose length represents the cylinder diameter corresponds to two velocity units in (*a*) and to one in (*b*). The normal velocity component $(0, 0, w)$ of the eigenmode vanishes identically in the $z = 0$ plane.

numbers considered and all wavenumbers. Similarly, the three-dimensional growth rate $\sigma_1^{(3D)}$ is – within the numerical accuracy – always smaller than the two-dimensional one $\sigma_1^{(2D)}$. Hence, the first group of dangerous three-dimensional eigenvalues form curves which are parametrized by k_z and terminate in the dangerous two-dimensional pair $\lambda_{1,2}^{(2)}$ for $k_z \to 0$. Therefore the onset of periodicity for $Re > Re_{crit}$ is generally not a two-dimensional process but is accompanied by a *continuum* of growing three-dimensional disturbances. Such a continuum of unstable three-dimensional eigenmodes has also been discovered by Triantafyllou (1990) in a three-dimensional stability analysis of a parallel shear flow. In this analysis, the three-dimensional modes are associated with an unstable two-dimensional eigenmode in the limit $k_z \to 0$. Triantafyllou also proved that the three-dimensional modes must have a lower growth rate than the associated two-dimensional mode – in agreement with our numerical data for $\sigma_1^{(3D)}$ and $\sigma_1^{(2D)}$.

Figure 6 visualizes the temporal evolution of such a three-dimensional eigenmode for $k_z = 0.5$ and $Re = 100$. This originally normalized eigenmode has been multiplied by the arbitrary factor of 2 using the same criterion as for figure 4. Interestingly, the column (*b*) of this figure displays vortices on the x-axis with alternating sign, which

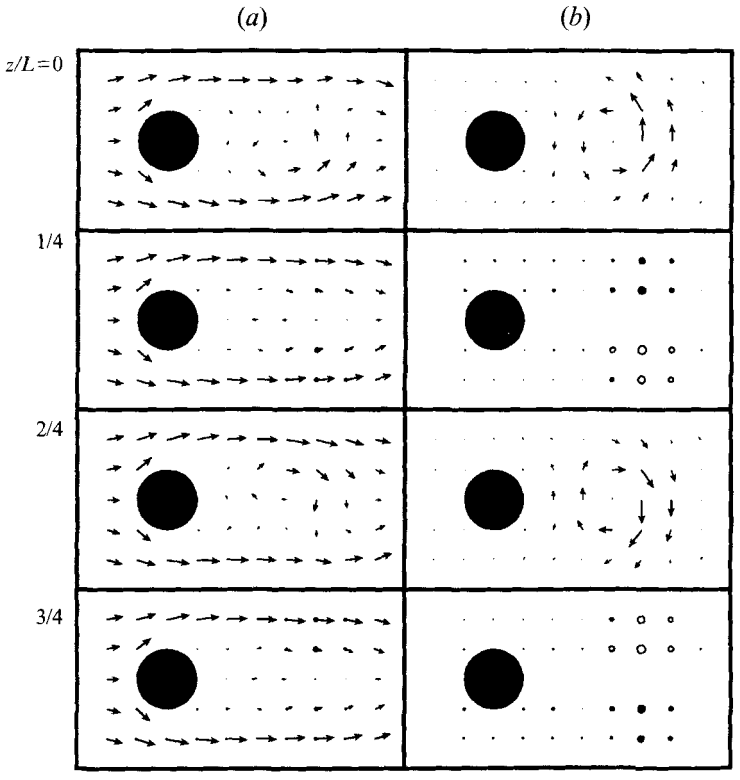

FIGURE 7. Same eigenmode as in figure 6 but visualized for $t = 0$ and in the planes $z/L = 0, \frac{1}{4}, \frac{2}{4}$, and $\frac{3}{4}$. The arrows have the same meaning as in figure 6. The diameter of the circles is half the normal velocity magnitude $|w|$ in the (a) and twice as much in (b). A circle is solid for $w > 0$ and open otherwise.

convect downstream. This flow is very similar to the two-dimensional eigenmode presented in figure 4 for a lower Reynolds number. Superimposing this three-dimensional eigenmode on the steady solution, a von Kármán vortex street is obtained in column (a) of figure 6. From figure 7 the three-dimensional eigenmode can be inferred as two local shedding cells centred at the $z = 0$ and $z = \frac{1}{2}L$ planes with opposite phase. These shedding cells are separated by planes $z = \text{const}$ in which the u, v components identically vanish and the cells 'communicate' only with a non-vanishing w flux. These local shedding cells are associated with a pair of two counter-rotating vortices oriented in a downward direction as can be seen from figure 8. The qualitative structure of the eigenmode of $\lambda_{1,2}^{(3D)}$ does not significantly depend on the Reynolds number or the wavenumber. These vortex pairs were also seen in experimental flow-visualizations for $Re = 200$ by König (1993).

The second group of dangerous three-dimensional eigenvalues is given by $\lambda_1^{(3D)} = \pi\sigma_1^{(3D)} > 0$ (see last column in figure 5c). The corresponding eigenmode is shown in figures 9 and 10. This mode introduces alternately a backward and forward flow in the near wake (see figure 9). The back view in figure 10 displays a quadrupol-like structure of the v, w components in the near wake. It should be noted that this eigenmode only introduces a three-dimensionality but not a new frequency to the perturbations of the steady solution.

This group of positive eigenvalues assumes its maximal growth rates for $k_z \approx 1.75$ and for $Re > 170$. Interestingly, detailed numerical investigations reveal that this real

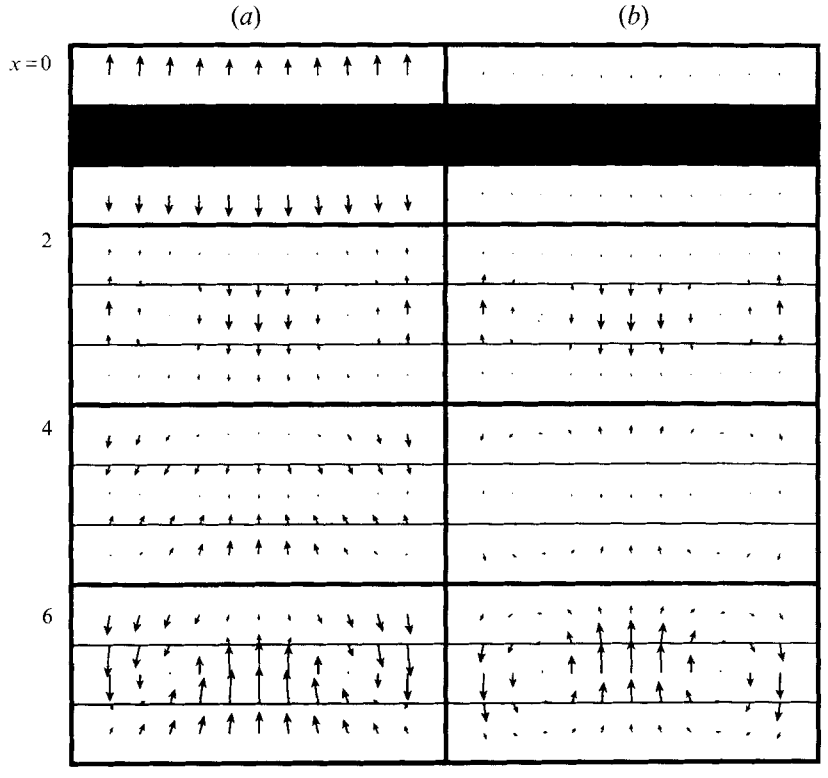

FIGURE 8. Same eigenmode as in figure 6, but visualized for $t = 0$ and in the planes $x = 0$, 2, 4 and 6. The arrows illustrating the tangential velocity component $(0, v, w)$ with respect to the view plane $x = \text{const}$ are twice as large as in figures 6 and 7, i.e. their lengths are $(v^2 + w^2)^{\frac{1}{2}}$ in the (a) and $2(v^2 + w^2)^{\frac{1}{2}}$ in (b). The visualization of the velocity component $(u, 0, 0)$ normal to the $x = \text{const}$ planes by circles is omitted in this figure.

eigenvalue only assumes a positive growth rate when the corresponding Floquet analysis of the periodic solution (with the same Re- and k_z-values) indicates a three-dimensional instability of the two-dimensional periodic flow (see §4.2). This correlation between stability and Floquet analyses is – at first sight – very surprising. This coincidence implies that small three-dimensional perturbations of the steady flow, which are described in the framework of the linear stability theory, already 'feel' the three-dimensionality of the asymptotical solution, to which they finally converge. This link makes the correlation between the stability and Floquet analyses plausible. In fact, neither the real eigenvalue $\lambda_1^{(3D)} > 0$ nor the corresponding real Floquet multiplier $\mu_1^{(3D)} > 1$ (see figure 15) introduce a new frequency to the cylinder wake and the asymptotical flow is strictly periodic in a small-Reynolds-number interval after the onset of three-dimensionality. This shows that global stability analyses of unstable steady flows may be very powerful tools for predicting a variety of features of the corresponding asymptotical flows.

3.3. *Evolution of finite disturbances*

In §3.1 the onset of two-dimensional vortex shedding is shown to be caused by a Hopf bifurcation. Provansal *et al.* (1987) and Sreenivasan, Strykowski & Olinger (1987) experimentally observed that the transient flows for $Re \approx Re_{crit}$ are well described by Landau's model (see Landau & Lifshitz 1987) for a supercritical Hopf bifurcation. In

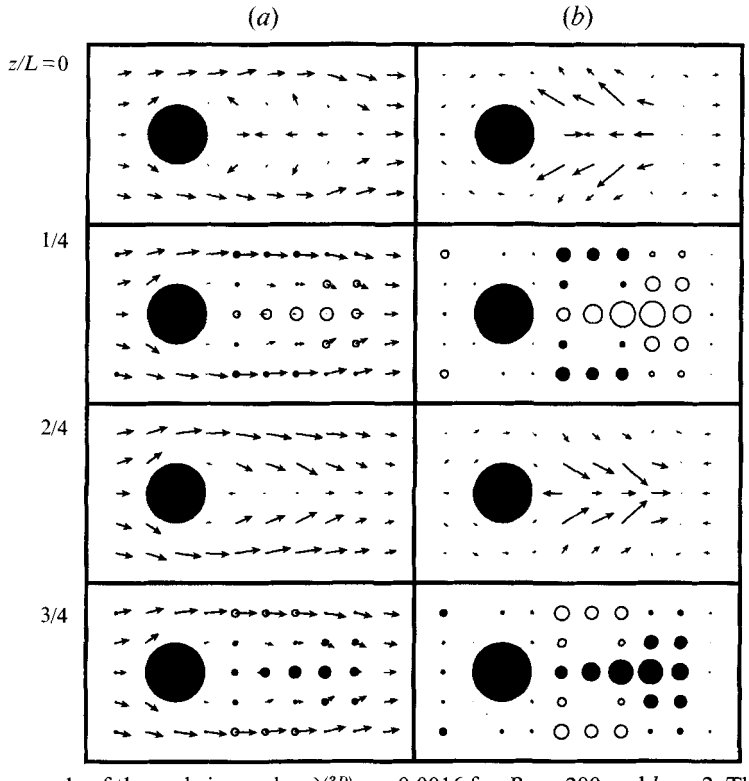

FIGURE 9. Eigenmode of the real eigenvalue $\lambda_1^{(3D)} = \pi 0.0016$ for $Re = 200$ and $k_z = 2$. This eigenmode is also multiplied by 3.5 and visualized in the same manner as the mode in figure 7.

this section the validity of the Landau model is numerically investigated. Three-dimensional disturbances are neglected.

Landau proposed a simple approximate description of small transient disturbances in the neighbourhood of a supercritical Hopf bifurcation. Let $\boldsymbol{u}^{(s)}(\boldsymbol{x})$ be the steady flow and $\boldsymbol{u}^{(e)}(\boldsymbol{x})$ be the eigenfunction (see figure 4) corresponding to the dangerous complex-conjugated eigenvalue pair $\lambda_{1,2} = \pm \mathrm{i}\omega$ at $Re = Re_{crit}$. Then the time-dependent perturbation $\boldsymbol{u}' = \boldsymbol{u} - \boldsymbol{u}^{(s)}$ is approximately given by the real part of $A\,\mathrm{e}^{\mathrm{i}\phi}\boldsymbol{u}^{(e)}$, where A denotes a slowly varying real amplitude and ϕ a time-dependent phase of the oscillation. The temporal evolution of these quantities for $Re \approx Re_{crit}$ is described by

$$\frac{\mathrm{d}}{\mathrm{d}t}A = \sigma A - \beta A^3, \tag{18}$$

$$\frac{\mathrm{d}}{\mathrm{d}t}\phi = \omega + \gamma A^2, \tag{19}$$

$$\sigma = \alpha(Re - Re_{crit}), \tag{20}$$

where the amplification-rate σ, the (non-normalized) real part of $\lambda_{1,2}$, is assumed to vary linearly with Re with the proportionality constant α. The effect of the nonlinear terms is described by the positive damping constant β and the frequency-deviation parameter γ, both of which are considered to be independent of the Reynolds number.

The set of parameters, ω, α, β, δ, which completely specifies the Landau model, may be normalized in different ways. The values which result from a non-dimensionalization with the velocity U_{crit} (corresponding to Re_{crit}) and the cylinder radius R – like in the

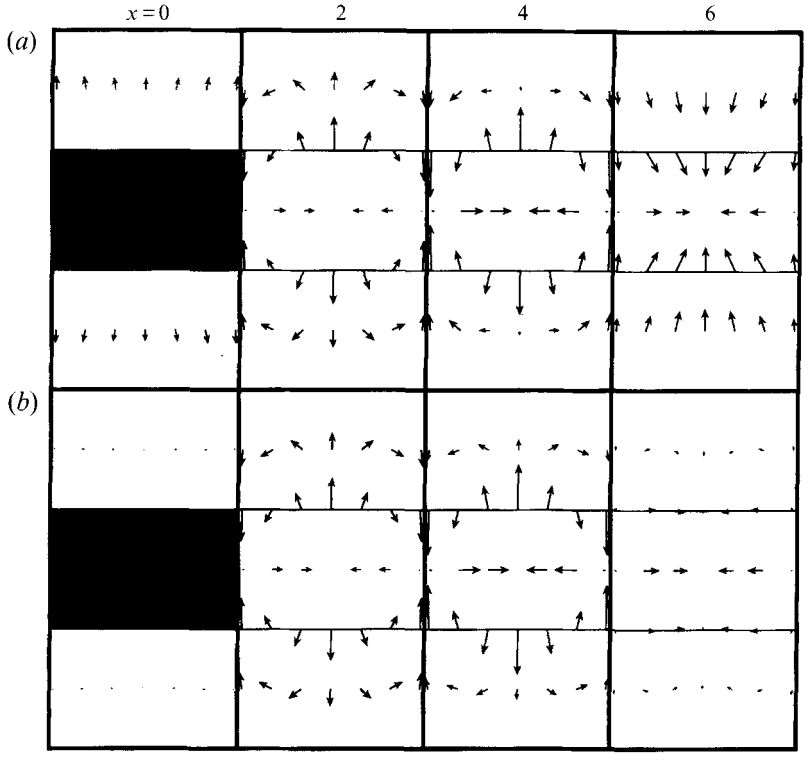

FIGURE 10. Same eigenmode as in figure 9, but visualized in the planes $x = 0$, 2, 4, and 6. Row (*b*) displays the eigenmode, whereas in (*a*) the steady flow is added to this mode. The arrows are aligned with the tangential velocity component $(0, v, w)$ with respect to the view planes $x = \text{const}$. Their lengths are $(v^2 + w^2)^{\frac{1}{2}}$ in both (*a*) and (*b*). The u-component is not illustrated in this figure.

Galerkin method – are denoted by the superscript (n) (for numerical). If the normalization quantities are U_{crit} and the cylinder diameter D, the corresponding superscript is (c) (for convection). When D and the kinematic viscosity ν are used, the non-dimensionalized quantities or denoted with the superscript (d) (for dissipation). These three sets of non-dimensionalized parameters are related via

$$\frac{\omega^{(c)}}{\omega^{(n)}} = \frac{\alpha^{(c)}}{\alpha^{(n)}} = \frac{\beta^{(c)}}{\beta^{(n)}} = \frac{\gamma^{(c)}}{\gamma^{(n)}} = 2, \tag{21}$$

$$\frac{\omega^{(d)}}{\omega^{(c)}} = \frac{\alpha^{(d)}}{\alpha^{(c)}} = \frac{\beta^{(d)}}{\beta^{(c)}} = \frac{\gamma^{(d)}}{\gamma^{(c)}} = Re_{crit}. \tag{22}$$

In the following, the parameters of the Landau model are computed with the stability analysis and the asymptotical periodic solutions $\boldsymbol{a}^{(p)}$ of the autonomous system (14). With $St_{crit} = 0.149$ the onset frequency is given by $\omega^{(c)} = 2\pi St_{crit} = 0.936$. In order to determine α, the growth rates σ_1 are numerically computed for various Reynolds numbers around Re_{crit} (figure 11*a*). The slope for the least-square line displayed for the σ_1–Re relationship is given by $(1.27 \pm 4) \times 10^{-3}$. The S-shaped deviation of the $\sigma_1(Re)$ data from the least-square line in figure 11 seems to be a truncation-error effect of the present Galerkin method, since it has not been found with the other Galerkin methods mentioned in §2.1. Noting that $\sigma^{(c)} = \pi\sigma_1$, we obtain

$$\alpha^{(c)} = 0.00399.$$

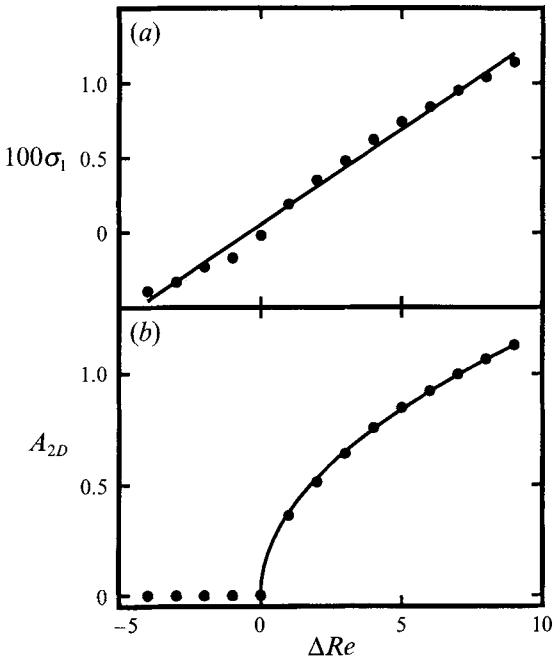

FIGURE 11. Growth rate and amplitude of oscillation in the neighbourhood of Re_{crit}. In (*a*) the numerically computed values for the growth rate σ_1 in terms of the Reynolds-number difference $\Delta Re = Re - Re_{crit}$ is illustrated with solid circles. The straight line is a least-square fit through the displayed $(\Delta Re, \sigma_1)$ points. In (*b*) the amplitude of the oscillation is shown in terms of ΔRe. This amplitude is defined by (24). The parabola curve is a least-square fit through the $(\Delta Re, A_{2D})$ points shown, with $\Delta Re \geqslant 0$.

In order to determine the damping constant $\beta^{(c)}$, the asymptotic amplitude A_{2D} is derived from (18) and (19):

$$A_{2D} = \left(\frac{\alpha}{\beta}\right)^{\frac{1}{2}} (Re - Re_{crit})^{\frac{1}{2}}. \tag{23}$$

For $Re > Re_{crit}$ we define the saturated amplitude of oscillation A_{2D} to be the time-averaged distance of the periodic trajectory $t \mapsto \boldsymbol{a}^{(p)}$ to the fixed point $\boldsymbol{a}^{(s)}$, i.e.

$$A_{2D} = \frac{1}{T} \int_0^T \mathrm{d}t \left[\sum_i (a_i^{(p)} - a_i^{(s)})^2 \right]^{\frac{1}{2}}, \tag{24}$$

where $T = 2/St$ is the period in terms of R/U units. This quantity can be shown to be proportional to the velocity amplitudes at any point in the wake region for $Re = Re_{crit}$. Figure 11(*b*) clearly displays the square-root dependency between the numerically obtained amplitude A_{2D} of the Galerkin method and the Reynolds-number difference $Re - Re_{crit}$. A least-squares fit yields $A_{2D} = (0.376 \pm 0.009)(Re - Re_{crit})^{\frac{1}{2}}$. With (23) the damping constant is computed to be

$$\beta^{(c)} = 0.0282.$$

For the computation of $\gamma^{(c)}$, the relationship between the asymptotic Strouhal number St_{2D} and Re is derived from (19) and (23):

$$St_{2D} - St_{crit} = \frac{\gamma^{(c)} \alpha^{(c)}}{2\pi \beta^{(c)}} (Re - Re_{crit}). \tag{25}$$

This linearity is confirmed by the numerical data presented in figure 12, the slope is

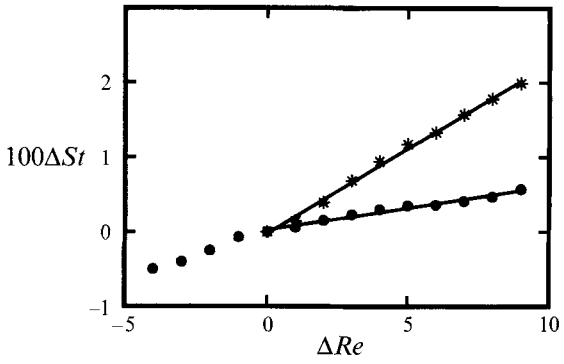

FIGURE 12. Strouhal-number differences $St_{2D} - St_{crit}$ and $St_1 - St_{crit}$ in the neighbourhood of Re_{crit}. The solid circles represent numerically obtained values of St_1 in terms of Re whereas the stars refer to the Strouhal number St_{2D} of the asymptotical periodic solution. The straight lines are least-square fits for both groups of Strouhal-number values using only the displayed data.

calculated with a least-square fit to be $(2.27 \pm 0.05) \times 10^{-3}$. With (25) and the already known parameters, the frequency deviation is found to be described by

$$\gamma^{(c)} = 0.103.$$

To compare these results with other publications, we transform the above parameters via (22):

$$\omega^{(d)} = 50.5, \quad \alpha^{(d)} = 0.215, \quad \beta^{(d)} = 1.52, \quad \gamma^{(d)} = 5.59.$$

The onset frequency $\omega^{(d)}$ has been compared with experimental and numerical investigations of other authors in §3.1. The $\alpha^{(d)}$-value is in very good agreement with 0.2 of Provansal *et al.* (1987) and of Sreenivasan *et al.* (1991). The $\beta^{(d)}$- and $\gamma^{(d)}$-values depend on the choice of the reference amplitude and cannot be compared with the experimental values. The ratio $\gamma^{(d)}/\beta^{(d)}$ is independent of the scaling of the amplitude; the predicted ratio of 3.68 is closer to the value 2.9 of Sreenivasan *et al.* than to the value of 0 of Provansal *et al.* (Note that $\frac{1}{2}l_r = \beta^{(d)}$ and $\frac{1}{2}l_i = -\gamma^{(d)}$ in Sreenivasan *et al.*'s and Provansal *et al.*'s notation. Hence $l_i/l_r = -\gamma^{(d)}/\beta^{(d)}$.)

The Landau model has been shown to be a good description for the onset of the two-dimensional vortex shedding. However, the validity of this model is restricted to two-dimensional perturbations although the continuum of three-dimensional eigenmodes has been shown to be of equal importance in §3.2. These three-dimensional effects may be incorporated in a Ginzburg–Landau equation which has been successfully applied by Albarède, Provansal & Boyer (1990), Albarède & Monkewitz (1992) and other authors to model vortex formations behind a circular cylinder.

4. Stability of the two-dimensional periodic flow

In this section results of the first global Floquet analysis of the two-dimensional periodic cylinder wake are presented. This analysis has been made possible by finding a low-dimensional Galerkin method for the three-dimensional flow. In §§4.1 and 4.2 the evolution of infinitesimal two-dimensional and three-dimensional disturbances is described. In §4.3 nonlinear effects on self-amplified finite perturbations are considered.

4.1. *Two-dimensional Floquet analysis*

In the two-dimensional Floquet spectra (see figure 13) the multipliers remain inside the unit circle for all Reynolds numbers considered. The spectral radius of the Floquet spectra, i.e. $|\mu_1^{(2D)}|$, is typically 0.60 ± 0.05. In other words the amplitude of a

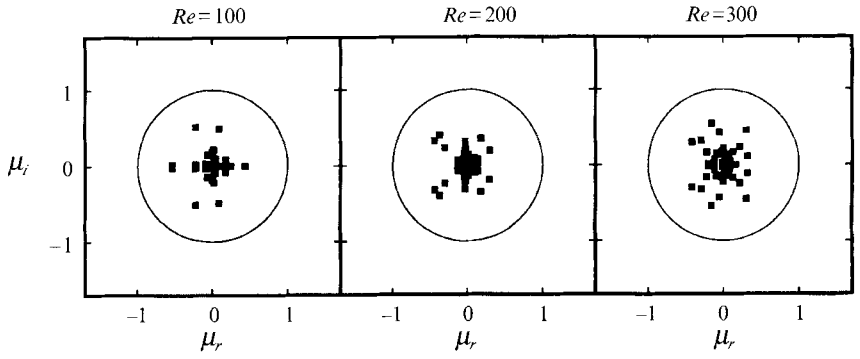

FIGURE 13. Two-dimensional Floquet spectra of the periodic solution for $Re = 100$, 200, and 300. Each solid square represents one multiplier $\mu_l^{(2D)} = \mu_{r,l}^{(2D)} + \mathrm{i}\mu_{i,l}^{(2D)}$.

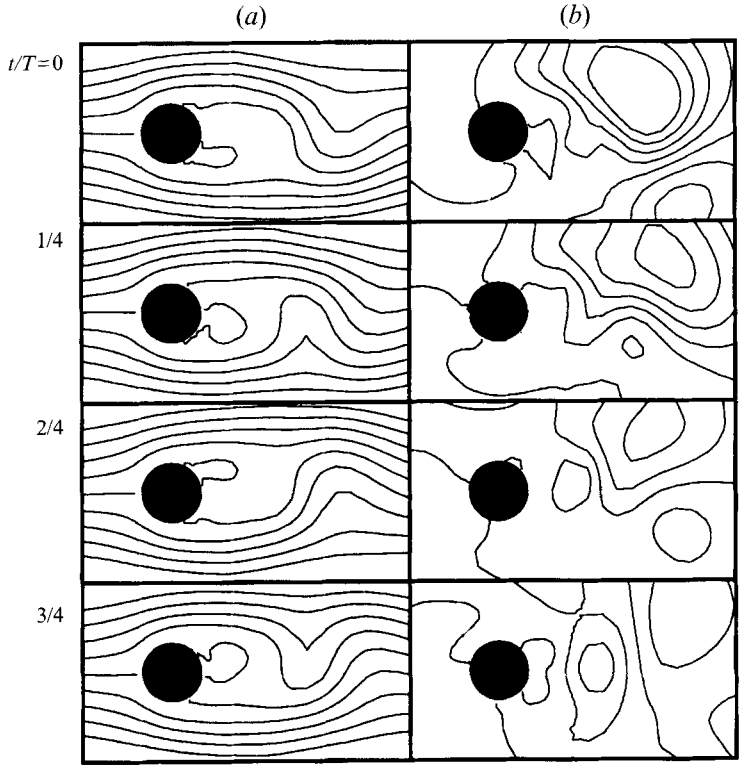

FIGURE 14. Floquet mode of the complex-conjugated multiplier pair $\mu_{1,2}^{(2D)} = -0.222 \pm \mathrm{i}0.517$ for $Re = 100$. Column (*a*) displays the streamlines of the periodic flow; column (*b*) illustrates the Floquet mode.

perturbation is reduced by approximately a factor of 0.6 per period – neglecting the phase shift on the limit cycle. Hence, the two-dimensional periodic flow is asymptotically stable with respect to two-dimensional disturbances. This stability was to be expected from the two-dimensional numerical simulations of Patel (1978) which yielded strictly periodic flows up to a Reynolds number of 500.

The present Floquet analysis has a variety of implications for the effect of periodic excitations on the cylinder wake for the regular Reynolds number regime

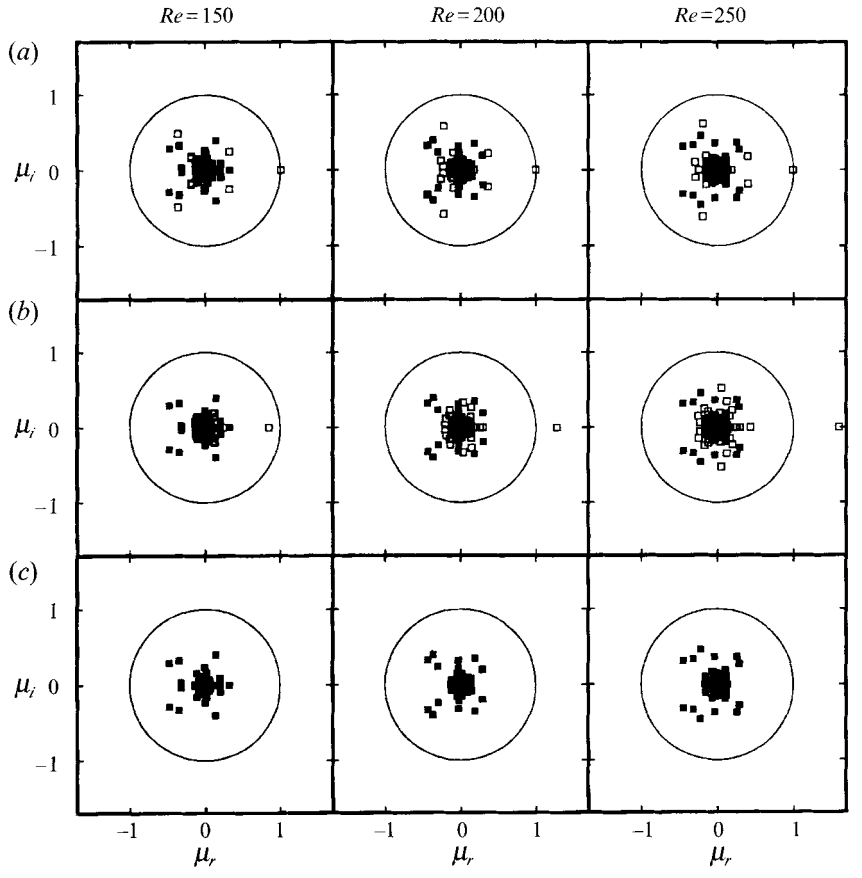

FIGURE 15. Floquet spectra of the periodic solution for $Re = 150$, 200, and 250 and for (*a*) $k_z = 0.1$, (*b*) 1.75 and (*c*) 3.0. Each solid square represents one two-dimensional multiplier $\mu_l^{(2D)} = \mu_{r,l}^{(2D)} + \mathrm{i}\mu_{i,l}^{(2D)}$, whereas the open symbols refer to three-dimensional ones $\mu_l^{(3D)} = \mu_{r,l}^{(3D)} + \mathrm{i}\mu_{i,l}^{(3D)}$.

$50 < Re < 175$. First, the excitation must be large in order to maintain significant deviations from natural vortex shedding, since all perturbations are strongly damped. This expectation is confirmed by the sound excitation experiments of Detemple-Laake & Eckelmann (1989). Secondly, one should expect a large variety of different excited vortex streets depending on the kind and amplitude of oscillation since there is no single dangerous real multiplier with $|\mu_1^{(2D)}| \gg |\mu_2^{(2D)}| \geqslant \ldots$ or a multiplier pair $|\mu_{1,2}^{(2D)}| \gg |\mu_3^{(2D)}| \geqslant \ldots$, but many multipliers with $|\mu_l^{c2D)}| \sim |\mu_1^{(2D)}|$. In fact, Detemple-Laake & Eckelmann (1989) could experimentally distinguish 12 topologically different kinds of periodically forced vortex streets. Thirdly, the structure of the excited perturbations may be inferred from the Floquet modes (or linear combinations thereof). Figure 14 displays the most dangerous Floquet mode for $Re = 100$. This mode represents a vortex formation which slowly convects downstream. Superimposing this mode on the vortex street with a speed of some 0.85 leads to beating phenomena in the local velocity amplitude. This was also found by Detemple-Laake & Eckelmann (1989).

4.2. *Three-dimensional Floquet analysis*

In this section the evolution of three-dimensional perturbations on the periodic cylinder wake is investigated employing the Floquet analysis. Figure 15 displays the Floquet spectra for three Reynolds numbers $Re = 150$, 200, and 250 and three

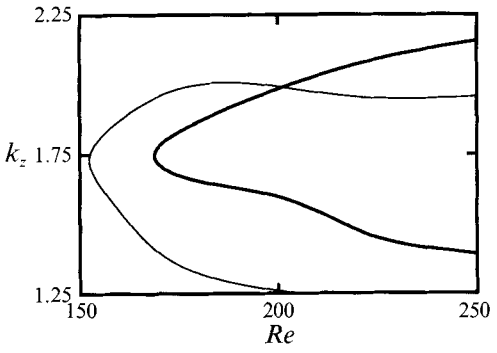

FIGURE 16. Stability diagram for the onset of three-dimensionality. The thick curve represents the neutral stability curve in terms of Re and k_z for the standard Galerkin method. In addition, a neutral stability curve (thin line) for the very low-dimensional $\mathscr{H}^{(+)}_{4,2,1}$ Galerkin method is included for comparison. Both stability curves are interpolated from 25 Floquet spectra for Re and k_z values which are integral multiples of 25 and 0.25, respectively.

spanwise wavenumbers $k_z = 0.1$, 1.75, and 3.0. Each Floquet spectrum consists of a k_z-independent two-dimensional contribution, discussed in the previous section, and k_z-dependent three-dimensional multipliers. For large spanwise wavenumbers (here $k_z = 3$), i.e. small wavelengths, the three-dimensional contribution lies in a small neighbourhood around the origin (covered by the two-dimensional spectrum in figure 15). This means that spanwise structures which are small as compared with the cylinder diameter are rapidly dissipated by viscosity for all Reynolds numbers considered. This dissipation effect explains why experimental flow visualizations do not show spanwise structures which are small compared to the cylinder diameter in the regular and transitional Reynolds number range.

For small wavenumbers (here $k_z = 0.1$), i.e. large wavelengths, such a dissipation mechanism is lacking and the spectral radius $|\mu_1^{(3D)}|$ is numerically observed to converge to unity for $k_z \to 0$. This implies that the two-dimensional periodic flow is only neutrally stable with respect to large-scale vortex deformations. This neutral instability is found for Reynolds numbers in the regular and transitional range. In experimental flow realizations, the end conditions may hence be expected to 'excite' these neutrally stable large-scaled vortex deformations in the regular Reynolds-number regime – in agreement with the observation of Chevron patterns, slanted vortex shedding, etc. (Williamson 1989; König *et al.* 1990; Hammache & Gharib 1991). Yet this interpretation of the theoretical results must be viewed with caution, since the detailed characteristics of the Floquet spectrum are certainly different for the periodic boundary condition assumed in the spanwise direction compared to the spectrum for vortex shedding behind a finite cylinder bounded by two end planes.

The distinguished non-vanishing finite wavenumber is $k_{z_{crit,2}} = 1.75$, corresponding to a wavelength of 1.80 diameters. For this wavenumber the onset of exponentially growing three-dimensional perturbations is observed for the lowest Reynolds number of $Re_{crit,2} = 170$. This onset of three-dimensionality is caused by a positive Floquet multiplier leaving the unit circle (see figure 15*b*). Figure 16 shows the corresponding neutral stability curve (thick line) in terms of the Reynolds number and spanwise wavenumber. For all (Re, k_z) values on this curve, the positive Floquet multiplier just crosses the unit circle. The wavenumbers k_z of amplified perturbations lie inside the thick tongue-shaped stability curve for a given Reynolds number.

Summarizing, the Floquet analysis predicts an absolute three-dimensional instability

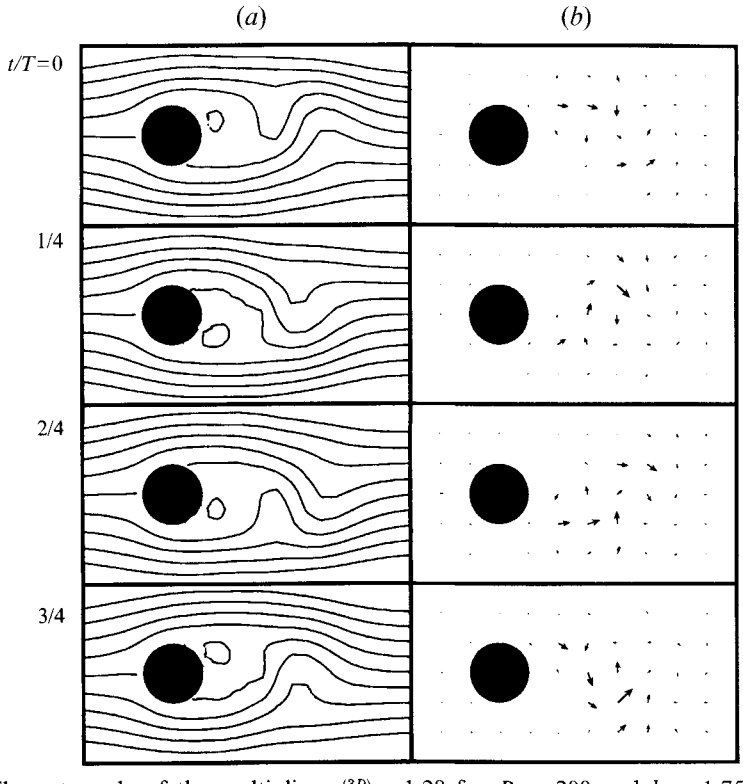

FIGURE 17. Floquet mode of the multiplier $\mu_1^{(3D)} = 1.28$ for $Re = 200$ and $k_z = 1.75$. Column (*a*) displays the periodic solution and column (*b*) illustrates the velocity field of the Floquet mode in the $z = 0$ plane for the instants $t/T = 0, \frac{1}{4}, \frac{2}{4}$, and $\frac{3}{4}$. This mode has been multiplied by the arbitrary factor 2 after the normalization. The lengths of the arrows are $(u^2+v^2)^{\frac{1}{2}}$.

which introduces a spanwise waviness of the von Kármán vortices for $Re > Re_{crit,2}$ and $k_{z_{crit,2}} = 1.75$. These three-dimensional fluctuations have been experimentally observed by Hama (1957), Williamson (1988*b*) and many other authors. The critical Reynolds number of 170 agrees well with Williamson's (1988*b*) value of 178. Also the spanwise wavelength of 1.8 diameters deviates by less than 10% from the value of 1.7 diameters experimentally obtained by Noack, König & Eckelmann (1993) with a smoke-wire technique. Karniadakis & Triantafyllou (1992) choose a similar wavenumber of $k_z = 2$ corresponding to a wavelength of $\frac{1}{2}\pi$ diameters in their numerical simulations. For this wavelength they observed an asymptotically stable three-dimensional flow for $Re > 210$. The stability diagram (figure 16), predicts the transition at the slightly lower value of $Re = 205$ for $k_z = 2$, since the neutral curve intersects the $k_z = 2$ line at this Reynolds number. Hence, Karniadakis & Triantafyllou's and our results for the onset of three-dimensionality are in excellent agreement.

The critical Reynolds number Re_{crit} and $k_{z_{crit,2}}$ predicted by the present $\mathscr{H}^{(+)}_{6,4,1}$ Galerkin method deviate by only some 5% from the experimental values, while the theoretical Strouhal numbers significantly exceed the experimental results for $Re \sim 200$ (see figure 20). Even the much coarser $\mathscr{H}^{(+)}_{4,2,1}$ Galerkin method with only 75 (!) modes predicts an absolute three-dimensional instability associated with a positive Floquet multiplier. The predicted critical point, $Re_{crit,2} = 152$ and $k_{z_{crit,2}} = 1.71$, compares reasonably well with the experimental data. The corresponding neutral stability curve is the thin line in figure 16. This curve deviates considerably from the $\mathscr{H}^{(+)}_{4,2,1}$-curve in

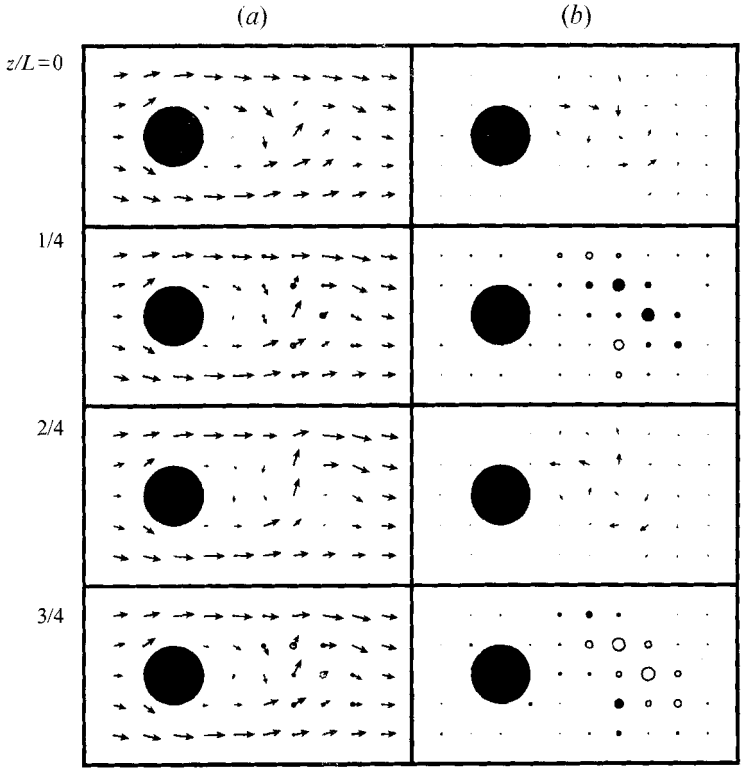

FIGURE 18. Same Floquet mode as in figure 17, but visualized for $t = 0$ and in the planes $z/L = 0$, $\frac{1}{4}$, $\frac{2}{4}$, and $\frac{3}{4}$. Column (*b*) shows the Floquet mode, and in column (*a*) this mode is superimposed on the periodic flow. The length of the arrows and radii of the circles are half the velocity component tangential and normal to the view plane $z = \text{const}$ in the (*a*) and twice as much in (*b*).

the same figure, particularly for $Re > 250$. This discrepancy is caused by the insufficient wake resolution of the coarse $\mathscr{H}^{(+)}_{4,2,1}$ Galerkin method. This method resolves only a part of the near wake, the numerical shedding frequency being some 20% too large. Hence, the transition process seems to be located in the near wake and appears to be rather insensitive to the temporal periodicity of two-dimensional vortex shedding. These circumstances explain why the three-dimensional Floquet analysis can be carried out with comparatively small maximal orders $I = 6$ and $J = 4$ for the radial and azimuthal modes. Naturally, an increase of the spanwise order $K = 1$ does not yield improved stability results, since the stability theory predicts that the z-dependency of the three-dimensional perturbations is incorporated in the complex factor $\exp(\mathrm{i}k_z z)$.

Another implication of the present Floquet analysis is that the onset of three-dimensionality does not introduce a further frequency to the flow, since the dangerous Floquet multiplier is real and positive. In fact, Karniadakis & Triantafyllou observe a periodic three-dimensional solution after the instability of the two-dimensional one. Their results are confirmed with the present Galerkin method.

To elucidate the mechanism behind the three-dimensional instability, the Floquet mode of $\mu_1^{(3D)}$ is visualized in figures 17, 18, and 19 for $Re = 200$ and $k_z = 1.75$. The velocity fluctuations of this mode are seen to be concentrated in the near wake, where the curvature of the streamlines and local centrifugal accelerations of the fluid particles are largest. At $z = 0$ the u, v components are mostly aligned with the periodic vortex shedding, whereas at $z = \frac{1}{2}L$ the mode generally interferes destructively with the von

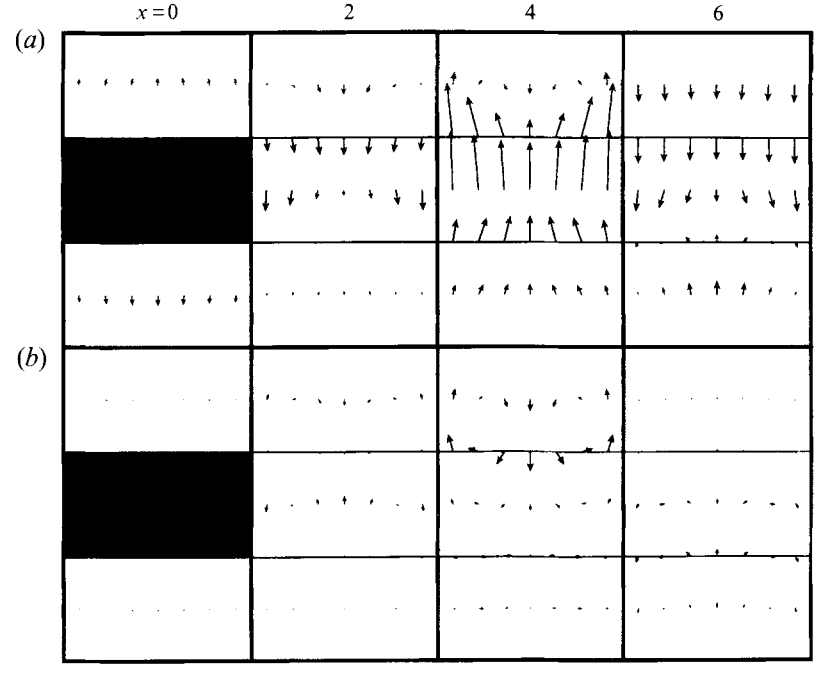

FIGURE 19. Same Floquet mode as in figure 18, but visualized for $t = 0$ and in the planes $x = 0$, 2, 4, and 6. Row (*b*) illustrates this mode; in row (*a*) the periodic solution is added. In both (*a*) and (*b*) the length of the arrows is $(v^2+w^2)^{\frac{1}{2}}$. The visualization of the velocity component u by circles is omitted in this figure.

Kármán vortex street (see figures 17 and 18). These shedding cells communicate through the planes $z = \frac{1}{4}L$ and $z = \frac{3}{4}L$ via a spanwise fluid transfer. In figure 19, the three-dimensional flow seems to be characterized by a vortex pair oriented in a downward direction.

The spatial structure of the Floquet mode suggests that the onset of three-dimensionality seems to be caused by a near-wake instability as opposed to a stagnation-line or Görtler-type boundary-layer instability and in contrast to a far-wake instability by slow self-amplified vortex deformations. Unfortunately, this mode is topologically too complex to estimate the $Re_{crit,2}$ or $k_{z_{crit,2}}$ from an already known instability process.

4.3. *Evolution of finite disturbances*

The Floquet analysis of §4.2 predicts for $Re > Re_{crit,2}$ and $k_z \approx 1.75$ an exponential growth of the infinitesimal disturbances around the limit cycle Γ_{2D} which represents two-dimensional vortex shedding. This linear stability theory, however, does not include nonlinear effects which prevent the explosions of finite disturbances. Simulations of the autonomous system (14) show that the trajectories starting near the unstable limit cycle converges to another limit cycle Γ_{3D} which corresponds to the three-dimensional periodic wake already investigated by Karniadakis & Triantafyllou (1992). In this section the transition from two-dimensional to three-dimensional vortex shedding is interpreted in the framework of the dynamical-system theory.

First we determine if the transition is soft or hard, i.e. occurs continuously or with a hysteresis in terms of the Reynolds number. For this purpose three observables are considered: the Strouhal numbers St_{2D} and St_{3D} for the limit cycles Γ_{2D} and Γ_{3D}

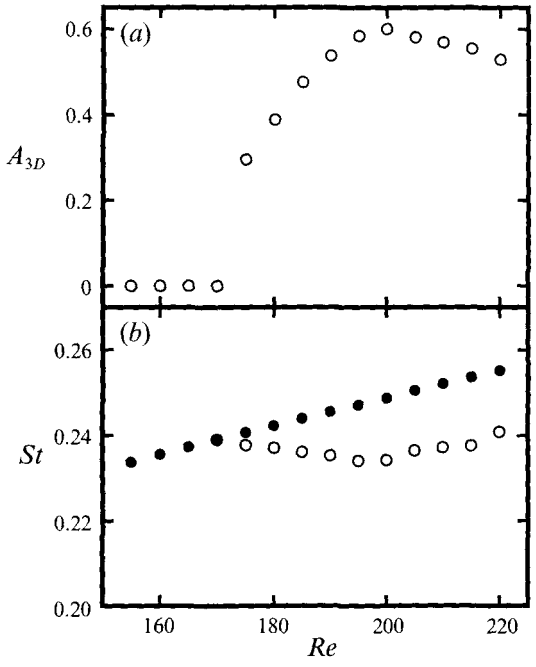

FIGURE 20. Amplitude of the three-dimensional fluctuations A_{3D} (see (26)) and Strouhal number St in terms of the Reynolds number. The solid (open) circles represent numerically obtained values of two-dimensional (three-dimensional) simulations.

respectively, and the time-averaged Euclidean distance A_{3D} of a trajectory $t \mapsto \boldsymbol{a}^{(p,3D)}$ on Γ_{3D} to the invariant subspace spanned by the two-dimensional Fourier coefficients $\{a^{(1)}_{ij0}\}_{\substack{i=0,\dots,I \\ j=-J,\dots,J}}$:

$$A_{3D} = \frac{1}{T}\int_0^T \mathrm{d}t \left[\sum_{i=\substack{\text{index of} \\ \text{3D mode}}} (a_i^{(p,3D)})^2 \right]^{\frac{1}{2}}. \tag{26}$$

These observables are numerically determined as a function of the Reynolds number for the critical wavenumber $k_z = 1.75$ and displayed in figure 20. The amplitude A_{3D} seems to be proportional to $(Re - Re_{crit,2})^{\frac{1}{2}}$, while the Strouhal numbers $St_{3D}(Re)$ seems to separate from $St_{2D}(Re)$ in a linear manner. It should be noted that a close analogy appears to exist between this bifurcation and the Hopf bifurcation discussed in §3.3. The quantities St_{2D}, St_{3D}, and A_{3D} of the three-dimensional instability behave similarly to the quantities St_1, St_{2D}, and A_{2D} in the temporal Hopf bifurcation. Hence, the investigations identify the onset of three-dimensionality in the periodic two-dimensional vortex shedding as a supercritical Hopf bifurcation with respect to the spanwise coordinate – in analogy to the onset of the convection rolls in the Rayleigh–Bénard problem. The periodic three-dimensional flow may therefore be bijectively mapped on a torus where one phase corresponds to the temporal periodicity, whereas the other (stationary) phase corresponds to a translation of the (periodic in the spanwise direction) velocity field $\boldsymbol{u}^{(p,3D)}$ along the cylinder axis. In §5.2 a generalized Landau model for this bifurcation is proposed. Karniadakis & Triantafyllou (1992) also observe a 'soft transition' towards a time-periodic three-dimensional flow.

The existence of a near wake which is periodic in time and in the spanwise coordinate is experimentally confirmed for $Re = 200$ by König (1993). In contrast to the numerical

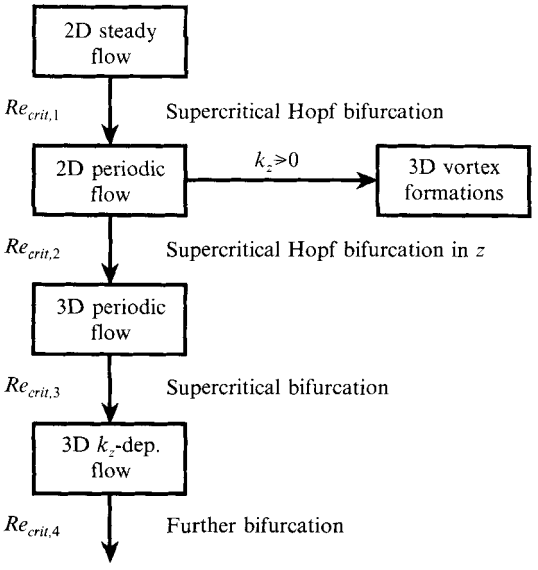

FIGURE 21. Proposed phenomenogram for the cylinder wake at low Reynolds numbers.

simulations, König reports irregular non-periodic fluctuations in the far wake for the same Reynolds number. This irregularity may be caused by the experimental realization of the end conditions.

According to Karniadakis & Triantafyllou (1992), the three-dimensional periodic solution becomes unstable in a period-doubling scenario for $k_z = 2$. Our Galerkin method confirms the period-doubling process with a strong frequency component at $\frac{1}{2}St_{3D}$ at $Re_{crit,4} = 285 \pm 5$ and $k_z = 1.75$. At $Re_{crit,3} = 198$, however, a temporal Hopf bifurcation is observed. This bifurcation may either be due to a different choice of the spanwise wavenumber, or it may be an artefact of the very low resolution $K = 1$ in the spanwise direction. With the available computer resources, no sensitivity analysis in terms of K can be carried out. In any case, the properties of the cylinder wake in terms of the Reynolds number for a given spanwise wavenumber can be summarized in figure 21.

Eventually, at sufficiently large Reynolds numbers, the cylinder wake is irregular. For $Re = 300$ our low-dimensional Galerkin method predicts a strange attractor with one positive Liapunov exponent and a fractal dimension of 3.4 (Noack & Eckelmann 1994*b*). Yet these simulations do not resolve fine-scaled structures. Chaos-theoretical evaluations of experimental velocity fluctuations yield a dominant dynamics with a similar correlation dimensional between 3 and 3.5 in the transitional Reynolds-number range superimposed by a low level of very high-dimensional stochastic noise (Noack 1990; Noack & Obermeier 1991).

5. Phenomenological models

In this section, the instability processes described in §§ 3 and 4 are modelled by simple dynamical systems. Some phenomena can already be understood in the framework of the Ginzburg–Landau equation (§ 5.1). In § 5.2 a generalization of the Landau model is proposed which incorporates the basic features of the first bifurcations.

5.1. *Ginzburg–Landau model*

The Ginzburg–Landau model has been successfully applied to describe vortex formations behind a cone (Papangelou 1992), behind a circular cylinder (Albaréde *et al.* 1990; Albaréde & Monkewitz 1992), and behind a torus (Leweke, Provansal & Boyer 1993). In this section, the prediction of the Ginzburg–Landau model with respect to perturbations with a spanwise periodicity is investigated.

Let us suppose that the vortex shedding in the near-wake region is described by a real amplitude A and a phase ϕ. A physical interpretation of this idealization is given by Noack, Ohle & Eckelmann (1991). Both quantities depend – in this idealization – only on the time t, and the spanwise coordinate z can be summarized in a complex amplitude $U = A\exp(\mathrm{i}\phi)$. The dynamics of the complex amplitude may be modelled by the Ginzburg–Landau equation

$$\partial_t U = (\sigma+\mathrm{i}\omega)\,U-(\beta+\mathrm{i}\gamma)|U|^2U+\kappa\,\partial_{zz}\,U, \tag{27}$$

where σ, β, γ and ω are real parameters and κ represents a real or complex coupling constant. The operators ∂_t and ∂_{zz} denote the first time and second z derivatives, respectively.

For $\kappa = 0$, (27) is equivalent to the real Landau equations (18) and (19) and the parameters σ, β, γ and ω have the same meaning. Yet, it must be born in mind that the amplitude and phase in the original Landau theory are associated with the global two-dimensional eigenmode, whereas these quantities have only a local meaning in the Ginzburg–Landau model.

The coupling constant κ is generally adjusted to experimental data. The idealized near-wake model of Noack *et al.* (1991) yields $\kappa = \nu$. In reality, spanwise velocity fluctuations seem to induce a much larger diffusion in the spanwise direction than molecular diffusion. For circular cylinders, Leweke *et al.* (1993) and Albaréde & Monkewitz (1992) use $\kappa = (32-20.8\mathrm{i})\,\nu$. For slender cones, Papangelou (1992) assumes a real coupling constant of $\kappa = 279\nu$.† In the van der Pol model of Noack *et al.* (1991), the best agreement with experiments was found for a couping constant of around 324ν.

In the following, the stability of the periodic z-independent solution $U^{(p)}$ with respect to infinitesimal perturbations U' is investigated. The first variational form of (27) reads

$$\partial_t U' = (\sigma+\mathrm{i}\omega)\,U'-(\beta+\mathrm{i}\gamma)(U^{(p)^2}U'^*+2|U^{(p)}|^2U')+\kappa\,\partial_{zz}\,U',$$

where the asterisk denotes complex conjugation. The perturbation U' can be decomposed into a term V which satisfies the linearized complex Landau equation

$$\partial_t V = (\sigma+\mathrm{i}\omega)\,V-(\beta+\mathrm{i}\gamma)(U^{(p)^2}V^*+2|U^{(p)}|^2V),$$

and a quantity W which obeys the diffusion equation

$$\partial_t W = \kappa\,\partial_{zz}\,W.$$

The V-term is z-independent and represents a time-periodic phase shift on the limit cycle in the complex plane. This contribution neither vanishes nor explodes and is immaterial for our stability investigation. The W-term describes the spanwise waviness

† This value has been derived by the authors for '$\kappa_r = 250(\Delta z)^2$', assuming that Papangelou forgot the unit 'Hz' in the specification of the coupling constant. With $\kappa = 279\nu$, Papangelou's (1992) theoretical results could be reproduced.

with the wavenumber k_z. Without loss of generality, the solution can be factorized in the form

$$W = \text{constant} \times \exp(-\kappa k_z^2 t) \exp(\mathrm{i} k_z z).$$

Hence, the half-time $T_{\frac{1}{2}}$ for the spanwise perturbation is given by $T_{\frac{1}{2}} = -\ln \frac{1}{2}/(\kappa_r k_z^2)$. Non-dimensionalizing this equation with the approximate shedding period $T_{per} = 0.2D/U$ and using $k_z = 2\pi/L$, we obtain

$$\frac{T_{\frac{1}{2}}}{T_{per}} \approx 0.088 \frac{\nu}{\kappa_r} \left(\frac{L}{D}\right)^2 Re. \tag{28}$$

This equation describes qualitatively correctly the neutral stability for large spanwise wavelengths, i.e. $T_{\frac{1}{2}}/T_{per} \to \infty$ for $L/D \to \infty$. This stability property can easily be explained as a diffusion-time effect. The spanwise diffusion in the Landau equation requires roughly the time L^2/κ_r to 'synchronize' the vortex shedding in a cell of length L. Therefore, $T_{\frac{1}{2}}$ is proportional to L^2 and inversely proportional to κ_r in (28).

For $L = D$, $Re = Re_{crit,2} = 170$ and $\kappa_r = 32\nu$ (see Leweke *et al.* 1993) equation (28) yields a very rapid dissipation with $T_{\frac{1}{2}} \approx 0.46 T_{per}$. This large dissipation of spanwise perturbations with $L \leqslant D$ is in qualitative agreement with the results of the Floquet analysis. Small spanwise 'shedding cells' are therefore rapidly synchronized.

In contrast to the cylinder wake, however, the Ginzburg–Landau model does not exhibit exponentially growing three-dimensional perturbations for intermediate spanwise wavelengths and sufficiently large Reynolds numbers. This is not surprising, since the absolute three-dimensional instability in the cylinder wake is a highly three-dimensional process, which cannot be expected to be suitably modelled by the simple diffusion term in the Ginzburg–Landau equation.

5.2. *A low-dimensional model for the transition scenario*

In this section, the Landau equations (18)–(20) are generalized to include the basic dynamical features of the onset of three-dimensionality for the critical spanwise wavenumber $k_z = 1.75$. This generalization is purely phenomenological and will illustrate how the two- and three-dimensional instability processes may be coupled. The form of the proposed equation may be derived from suitable prerequisites employing analyticity assumptions, symmetry considerations, and Bogoliubov–Krylov-type approximations – much in analogy with Landau's derivation of his equations (see Landau & Lifshitz 1987).

Let A and ϕ be the amplitude and phase associated with the two-dimensional vortex shedding and defined in §3.3. Let B be a real amplitude of the three-dimensional eigenmode associated with the real eigenvalue $\sigma_1^{(3D)}$ of §3.2. Then, the generalized Landau model is proposed to be of the form

$$\frac{\mathrm{d}}{\mathrm{d}t} A = \sigma A - \beta A^3, \tag{29}$$

$$\frac{\mathrm{d}}{\mathrm{d}t} \phi = \omega + \gamma A^2 - \gamma_B B^2, \tag{30}$$

$$\frac{\mathrm{d}}{\mathrm{d}t} B = \sigma_B B - \beta_B B^3, \tag{31}$$

$$\sigma = \alpha(Re - Re_{crit}), \tag{32}$$

$$\sigma_B = \alpha_B(Re - Re_{crit,2}), \tag{33}$$

where the α, β, γ, ω, γ_B, α_B, β_B are assumed to be Reynolds-number independent parameters, and σ, σ_B are the Reynolds-number dependent growth rates. The parameters without the subscript B have the same meaning as in §3.3. The new parameters α_B, β_B are assumed to be positive. For the cylinder wake, γ_B turns out to be positive. For $B \equiv 0$, this three-dimensional autonomous system reduces to the Landau equations (18)–(20).

The solutions and bifurcations of (29)–(33) can easily be physically interpreted. In the following discussion, A, ϕ, B are considered to be cylindrical coordinates of a Cartesian three-dimensional space. The eigenvalues and Floquet multiplier refer, hence, to the system of differential equations in Cartesian coordinates.

$A = B = 0$ corresponds to the steady two-dimensional flow. The stability spectrum of this fixed point has a complex-conjugated pair of eigenvalues $\sigma \pm i\omega$, which induces the temporal Hopf bifurcation in the $B = 0$ plane at $Re = Re_{crit}$, and a real eigenvalue σ_B, which induces the instability of the $B = 0$ plane for $Re > Re_{crit,2}$ and which corresponds to $\sigma_1^{(3D)}$.

For $Re > Re_{crit}$, the $B = 0$ plane contains a limit cycle Γ, corresponding to the two-dimensional vortex shedding. The period shall be denoted by T. The Floquet spectrum of the periodic solution can easily be derived to be $+1$, $\mu_2 = \exp(-2\sigma T)$ and $\mu_3 = \exp(\sigma_B T)$. Here, the $+1$ multiplier represents the immaterial phase shift on the limit cycle. μ_2 has a modulus less than unity and represents as decaying perturbation in the $B = 0$ plane. This corresponds to the observation in §4.1 that the periodic vortex street is asymptotically stable with respect to all two-dimensional perturbations. The real multiplier μ_3 leaves the unit circle at $Re = Re_{crit,2}$ and causes the instability of the periodic solution in the $B = 0$ plane. This event models the onset of three-dimensionality. For $Re > Re_{crit,2}$, almost all trajectories converge to limit cycles $\Gamma_{\pm B}$ in the planes $B = \pm(\alpha_B/\beta_B)^{\frac{1}{2}}(Re - Re_{crit,2})^{\frac{1}{2}}$. Note that B has a similar meaning to A_{3D} in figure 20. This quantity also grows in proportion to the square root of the Reynolds-number difference $Re - Re_{crit,2}$. The angular frequency ω_B of $\Gamma_{\pm B}$ differs from the frequency ω_A of the limit cycle Γ in the $B = 0$ plane by $\omega_B - \omega_A = (\alpha_B \gamma_B/\beta_B)(Re - Re_{crit,2})$. Hence both frequencies deviate linearly in terms of $Re - Re_{crit,2}$. This is in complete analogy with St_{2D} and St_{3D} of figure 20.

The generalized Landau equations also illustrate the observed one-to-one correspondence (see §3.2) between the stability and the Floquet spectrum. In the neighbourhood of $Re_{crit,2}$, the model eigenvalues σ_3 satisfy $\mu_3 - 1 = \exp(\sigma_B T) - 1 \approx \sigma_B T = \sigma_3 T = \alpha_B T(Re - Re_{crit,2})$, i.e. μ_3 crosses the unit circle in the complex plane whenever σ_3 crosses the imaginary axis. Both events are correlated, since the instability of the $B = 0$ plane is modelled to be independent of the limit-cycle dynamics in this plane. Similarly, the three-dimensionality of the cylinder wake is caused by a physical process, which is not based on the von Kármán vortex street, but can be considered as an instability of a steady velocity field.

One word of caution is order. The proposed three-dimensional model contains only two stable limit cycles for $Re > Re_{crit,2}$. In the cylinder wake, however, there exists a continuum of stable three-dimensional periodic wakes just above $Re_{crit,2}$. These solutions are the same except for a translation ζ in the spanwise direction. Hence, the model should be enlarged by a fourth equation

$$\frac{\mathrm{d}}{\mathrm{d}t}\zeta = 0.$$

Then the original pitchfork bifurcation of B should be interpreted as a Hopf bifurcation towards a torus around Γ with a steady second phase ζ. The situation is

analogous to the pitchfork bifurcation of the Lorenz (1963) model, which describes the onset of the Rayleigh–Bénard convection rolls.

6. Discussion and conclusions

The first bifurcations of the cylinder wake in terms of the Reynolds numbers are investigated in the first global, three-dimensional stability analysis and interpreted in the framework of dynamical-systems theory.

The onset of two-dimensional vortex shedding is found to be a supercritical Hopf bifurcation which can be described by the Landau model. These theoretical results confirm Sreenivasan *et al.*'s (1987) and Provansal *et al.*'s (1987) experimental investigation. The predicted critical Reynolds number is $Re_{crit} = 54$, which exceeds the experimental value of $Re_{crit} = 47$. Yet the discrepancy can be significantly decreased by increasing the number of modes in the Galerkin method employed. The experimental and theoretical coefficients of the Landau model deviate by a few percent up to approximately 20%, depending on the coefficient. This difference is acceptable in view of the difficult experimental realization of the transients from the steady to the periodic cylinder wake and in view of the accuracy of the 63-dimensional Galerkin method used. The physical process behind the onset of vortex shedding is described by Ahlborn & Lefrançois (1994).

The onset of three-dimensionality in the two-dimensional von Kármán vortex street is identified as a supercritical Hopf bifurcation in the spanwise coordinate. For this instability, a generalized Landau model is proposed and is numerically verified. The resulting 'soft transition' toward a periodic, three-dimensional flow has also been observed in the numerical simulations of Karniadakis & Triantafyllou (1992). The absolute three-dimensional instability occurs at $Re_{crit,2} = 170$ and introduces a spanwise wavelength of $L_{crit,2} = 1.8D$. Both critical quantities, $Re_{crit,2}$ and $L_{crit,2}$, deviate only some 5% from recent experimental investigations of Williamson (1988*b*) and Noack *et al.* (1993). The physical process behind the onset of three-dimensionality seems to be located in the near-wake – as opposed to the stagnation-line or Görtler-type instability in the boundary-layer and in contrast to a far-wake process. Interestingly, the two-dimensionally unstable steady solution becomes three-dimensionally unstable at the same critical point $Re_{crit,2}$ and $L_{crit,2}$. Hence, the transition seems to result from time-independent wake properties. These wake properties must incorporate downward velocity gradients of the near-wake since Triantafyllou (1990) concludes for steady parallel shear flows 'that three-dimensionality in wakes does not appear spontaneously as a result of a three-dimensional absolute instability of the homogeneous flow'. Unfortunately, the topological structures of the three-dimensional eigenmodes are very complex and no simple physical model can be proposed for the transition in the present publication.

The Galerkin method confirms the existence of the period-doubling process discovered by Karniadakis & Triantafyllou (1992). Yet the spanwise resolution of our Galerkin method is limited by the available computer power and no definite conclusion regarding the bifurcations for $Re > Re_{crit,2}$ can be drawn. The stability diagram for the transition clearly shows that the assumed spanwise periodicity has a strong effect on the critical Reynolds number and may therefore also affect the kinds of bifurcation in the transition scenario.

In contrast to the theoretical investigations, Williamson (1988*b*), König, Noack & Eckelmann (1993), and Brede *et al.* (1994) report a discontinuous frequency drop at $Re_{crit,2}$. This discrepancy may be induced by the experimental realization of the end

conditions which was found to be important for $Re_{crit} < Re < Re_{crit,2}$ – even for very large aspect ratios. These end conditions may induce perturbations which are not present in the numerical simulation. The discrepancy may also result from the periodic boundary conditions assumed in the spanwise direction. These kinds of condition may exclude the excitation of unstable three-dimensional perturbations which do not have the assumed wavelength. In this case, the boundary conditions would enforce a solution of the Navier–Stokes equation, which is unstable with respect to arbitrary perturbations and which can therefore not be observed experimentally. From the present experimental and numerical investigations, neither explanation can be conclusively verified or falsified.

The results of our global stability analysis explain a variety of experiments with periodically forced cylinders in the regular Reynolds-number range. For $Re < 25$, the stability spectrum has the features of a linear convection–dissipation system and contains no pronounced complex-conjugated eigenvalue pair. This explains Sreenivasan *et al.*'s (1991) experimental observation that no vortex shedding can be excited in this Reynolds-number range. For $Re_{crit} < Re < Re_{crit,2}$, the Floquet analysis shows that two-dimensional perturbations decay roughly by a factor of 0.6 during one shedding period. There exist a variety of Floquet modes with a similar amplification factor. Hence, the periodic forcing is expected to have a large amplitude, giving rise to a variety of different vortex shedding modes which depend strongly on the kind of the forcing. These expectations are confirmed by Detemple-Laake & Eckelmann's (1991) experiments, in which twelve different forced shedding modes are observed for a comparatively large acoustic excitation. Roussopoulos (1993) reports that vortex shedding can only be suppressed for Reynolds numbers up to 53, i.e. for a very narrow Reynolds-number range. This finding is not surprising in view of a continuum of unstable three-dimensional eigenmodes, which represent local vortex shedding cells.

The stability analysis also sheds some light on recent experimental studies of the laminar cylinder wake. The two-dimensional vortex shedding is found to be only neutrally stable with respect to three-dimensional perturbations for all Reynolds numbers considered. This neutral stability explains why laminar, parallel vortex shedding is experimentally very difficult to achieve. Small inhomogeneities in the experimental set-up easily give rise to large-scale deformations of the vortices, and these perturbations do not decay. Typically, chevron patterns and oblique shedding are experimentally observed unless particular end conditions are used (Williamson 1989; König *et al.* 1990, 1992; Hammache & Gharib 1991). In contrast, structures which are not larger than the cylinder diameter are predicted to decay rapidly and are not experimentally observed (Gerrard 1966).

Summarizing, the present investigation allows the interpretation of many experimental observations of the cylinder wake within the framework of a global stability theory. It also revealed an interesting relationship between the stability and Floquet theory.

We want to express our gratitude to Professor E.-A. Müller for his continuous interest in the work and for his provision of an excellent research environment. We acknowledge valuable discussions with Professors G. L. Brown, G. E. Karniadakis, and J. Sheridan. To R. Nolte and our wake team, namely M. Brede, U. Fey, F. Jacobitz, M. König, F. Ohle, and M. Weiland, we are indebted for many stimulating discussions.

Appendix A. Function systems for the Galerkin approximation

In this section the radial, azimuthal, and spanwise modes, $R_i^{(\kappa)}$, $\Phi_j(\phi)$, and $Z_k(z)$ are defined. The construction of these modes from mathematical completeness arguments and physical considerations is described by Noack (1992) and Noack & Eckelmann (1994*a*).

The *radial mode* $R_i^{(\kappa)}$ is the product of an exponentially decaying factor, a polynomial $P_i^{(\kappa)}$ of degree i, a slowly increasing factor $r^{+\frac{1}{4}}$ and a factor which guarantees the no-slip condition at the cylinder:

$$R_i^{(\kappa)} = \frac{1}{(\delta^{(\kappa)})^{\frac{1}{2}}} r^{+\frac{1}{4}} \left(\frac{r-1}{\delta^{(\kappa)}}\right)^{\kappa+1} P_i^{(\kappa)}\left(\frac{r-1}{\delta^{(\kappa)}}\right) \exp\left[-\left(\frac{r-1}{2\delta^{(\kappa)}}\right)\right]. \tag{A 1}$$

The scaling parameter $\delta^{(\kappa)}$ is given by

$$\delta^{(\kappa)} = \tanh\left[\frac{a^{(\kappa)}}{Re^{\frac{1}{2}}}\right], \tag{A 2}$$

where the constant $a^{(\kappa)}$ is determined from an estimate of the boundary-layer thickness:

$$a^{(\kappa)} = \begin{cases} 2.45 & \text{for} \quad \kappa = 1, \\ 2.95 & \text{for} \quad \kappa = 2. \end{cases} \tag{A 3}$$

The Reynolds-number-independent polynomials $P_i^{(\kappa)}$ are determined so that the radial modes satisfy the orthonormality relationship

$$\int_1^\infty \mathrm{d}r\, r^{-\frac{1}{2}} R_i^{(\kappa)}(r)\, R_l^{(\kappa)}(r) = \delta_{il}. \tag{A 4}$$

The system of *azimuthal modes* coincide with the trigonometric system for $Re \to 0$. With increasing Reynolds number the resolution in the wake region around $\phi = 0$ is increased, if the radial resolution I is larger than the azimuthal one J. The jth azimuthal mode is defined by

$$\Phi_j(\phi) = \begin{cases} \dfrac{1+\gamma\cos\phi}{\pi^{\frac{1}{2}}} \sin(jh(\phi)) & \text{for} \quad j > 0, \\ \dfrac{1+\gamma\cos\phi}{(2\pi)^{\frac{1}{2}}} & \text{for} \quad j = 0, \\ \dfrac{1+\gamma\cos\phi}{\pi^{\frac{1}{2}}} \cos(jh(\phi)) & \text{for} \quad j < 0, \end{cases} \tag{A 5}$$

where h represents the azimuthal coordinate transformation

$$h(\phi) = \phi + \gamma \sin\phi(1+\cos\phi) \tag{A 6}$$

and the distortion parameter γ is defined by

$$\gamma = \frac{I-J}{I} \tanh(Re/100). \tag{A 7}$$

For $J > I$, (A 7) is replaced by $\gamma = 0$, since $J > I$ already guarantees a good azimuthal resolution of the wake region.

The system of *spanwise modes* coincides with the complete, orthonormal trigonometric system for L-periodic functions except for the L-independent normalization factor:

$$Z_k(z) = \begin{cases} \frac{1}{\pi^{\frac{1}{2}}} \sin(2\pi kz/L) & \text{for} \quad k > 0, \\ \frac{1}{(2\pi)^{\frac{1}{2}}} & \text{for} \quad k = 0, \\ \frac{1}{\pi^{\frac{1}{2}}} \cos(2\pi kz/L) & \text{for} \quad k < 0. \end{cases} \tag{A 8}$$

Appendix B. Model equation for the spectrum at low Reynolds numbers

The linear convection–diffusion equation

$$\partial_t u + \partial_x u = \nu \partial_{xx} u,$$

roughly models the convection and dissipation of a perturbation u in the wake, x being the coordinate in the downstream direction; ν is the viscosity and corresponds to $1/Re$ in the linearized Navier–Stokes equation. This partial differential equation has the particular solution

$$u = \sin(k_x(x-t))\, e^{-\nu k_x^2 t},$$

which represents travelling decaying waves with the wavenumber k_x and the growth rate $\sigma = -\nu k_x^2$. The circular frequency ω for a fixed position x is related to the wavenumber by

$$\omega = k_x = (-\sigma/\nu)^{\frac{1}{2}}.$$

Hence, the frequency ω increases in proportion to the square-root of the (negative) growth rate σ. This ω–σ relationship qualitatively resembles the square-root dependency between St and σ of the outermost eigenvalues in figure 2.

REFERENCES

Ahlborn, B. & Lefrançois, M. 1994 The clockwork of vortex shedding. *Phys. Fluids* A (submitted).

Albarède, P. & Monkewitz, P. A. 1992 A model for the formation of oblique shedding patterns and 'chevrons' in cylinder wakes. *Phys. Fluids* A **4**, 744–756.

Albarède, P., Provansal, M. & Boyer, L. 1990 Modélisation par l'équation de Ginzburg–Landau du sillage tridimensionnel d'un obstacle allongé. *C.R. Acad. Sci. Paris* II **310**, 459–464.

Brede, M., Eckelmann, H., König, M. & Noack, B. R. 1994 Discrete shedding modes of the cylinder wake in a jet with a homogeneous core. *Phys. Fluids* A (submitted).

Busse, F. H. 1991 Numerical analysis of secondary and tertiary states of fluid flow and their stability properties. *Appl. Sci. Res.* **48**, 341–351.

Clever, R. M. & Busse, F. H. 1990 Convection at very low Prandtl numbers. *Phys. Fluids* A **2**, 334–339.

Detemple-Laake, E. & Eckelmann, H. 1989 Phenomenology of Kármán vortex streets in oscillatory flow. *Exps. Fluids* **7**, 217–227.

Gerrard, J. H. 1966 The three-dimensional structure of the wake of a circular cylinder. *J. Fluid Mech.* **25**, 143–164.

Hama, F. R. 1957 Three-dimensional vortex pattern behind a circular cylinder. *J. Aero. Sci.* **24**, 156–158.

Hammache, M. & Gharib, M. 1991 An experimental study of the parallel and oblique vortex shedding from circular cylinders. *J. Fluid Mech.* **232**, 567–590.

HUERRE, P. & MONKEWITZ, P. A. 1990 Local and global instabilities in spatially developing flows. *Ann. Rev. Fluid Mech.* **32**, 473–537.

JACKSON, C. P. 1987 A finite-element study of the onset of vortex shedding in flow past variously shaped bodies. *J. Fluid Mech.* **182**, 23–45.

JORDAN, D. W. & SMITH, P. 1988 *Nonlinear Ordinary Differential Equations*. Clarendon.

KARNIADAKIS, G. E. & TRIANTAFYLLOU, G. S. 1992 Three-dimensional dynamics and transition to turbulence in the wake of bluff bodies. *J. Fluid Mech.* **238**, 1–30.

KÖNIG, M. 1993 Experimentelle Untersuchung des dreidimensionalen Nachlaufs zylindrische Körper bei kleinen Reynoldszahlen. PhD thesis, Georg-August-Universität, Göttingen.

KÖNIG, M., EISENLOHR, H. & ECKELMANN, H. 1990 The fine structure in the Strouhal–Reynolds number relationship of the laminar wake of a circular cylinder. *Phys. Fluids* A **2**, 1607–1614.

KÖNIG, M., EISENLOHR, H. & ECKELMANN, H. 1992 Visualization of the spanwise cellular structure of the laminar wake of wall-bounded circular cylinders. *Phys. Fluids* A **4**, 869–872.

KÖNIG, M., NOACK, B. R. & ECKLEMANN, H. 1993 Descrite shedding modes in the von Kármán vortex street. *Phys. Fluids* A **5**, 1846–1848.

LANDAU, L. D. & LIFSHITZ, E. M. 1987 *Fluid Mechanics*. Pergamon.

LEWEKE, T., PROVANSAL, M. & BOYER, L. 1993 Sillage tridimensionnel d'un obstacle torique et modélisation par l'équation de Ginzburg–Landau. *C.R. Acad. Sci. Paris*, II **316**, 287–292.

LORENZ, E. N. 1963 Deterministic nonperiodic flow. *J. Atmos. Sci.* **20**, 130–141.

MORZYŃSKI, M. & THIELE, F. 1991 Numerical stability analysis of a flow about a cylinder. *Z. Angew. Math. Mech.* **71**, T424–T428.

NOACK, B. R. 1990 Untersuchung chaotischer Phänomene in der Nachlaufströmung. *Rep.* 111/1990. Max-Planck-Institut für Strömungsforschung, Göttingen.

NOACK, B. R. 1992 Theoretische Untersuchung der Zylinderumströmung mit einem niedrig-dimensionalen Galerkin–Verfahren. *Rep.* 25/1992. Mitteilungen des Max-Planck-Instituts für Strömungsforschung, Göttingen.

NOACK, B. R. & ECKELMANN, H. 1991 Two-dimensional, viscous, incompressible flow around a circular cylinder. *Rep.* 104/1991. Max-Planck-Institut für Strömungsforschung, Göttingen.

NOACK, B. R. & ECKELMANN, H. 1992 On chaos in wakes. *Physica D* **56**, 151–164.

NOACK, B. R. & ECKELMANN, H. 1993 Theoretical investigation of the cylinder wake with a low-dimensional Galerkin method. In *IUTAM-Symposium on Bluff Body Wakes, Dynamics, and Instability, Göttingen, 7–11 September 1992* (ed. H. Eckelmann, J. M. R. Graham, P. Huerre & P. A. Monkewitz), pp. 143–146. Springer.

NOACK, B. R. & ECKELMANN, H. 1994*a* A low-dimensional Galerkin method for the three-dimensional flow around a circular cylinder. *Phys. Fluids* **6**, 124–143.

NOACK, B. R. & ECKELMANN, H. 1994*b* Theoretical investigation of the bifurcations and the turbulence attractor of the cylinder wake. *Z. Angew Math. Mech.* **74**, T396–T397.

NOACK, B. R., KÖNIG, M. & ECKELMANN, H. 1993 Three-dimensional stability analysis of the periodic flow around a circular cylinder. *Phys. Fluids* A **5**, 1279–1281.

NOACK, B. R. & OBERMEIER, F. 1991 A chaos-theoretical investigation of the wake behind a cylinder. *Z. Angew. Math. Mech.* **71**, T259–T261.

NOACK, B. R., OHLE, F. & ECKELMANN, H. 1991 On cell formation in vortex streets. *J. Fluid Mech.* **227**, 293–308.

OERTEL, H. 1990 Wakes behind blunt bodies. *Ann. Rev. Fluid Mech.* **22**, 539–546, 1990.

PAPANGELOU, A. 1992 Vortex shedding from slender cones at low Reynolds numbers. *J. Fluid Mech.* **242**, 299–321.

PATEL, V. A. 1978 Kármán vortex street behind a circular cylinder by series truncation method. *J. Comput. Phys.* **28**, 14–42.

PRESS, W. H., FLAMERY, B. P., TEUKOLSKY, S. A. & VETTERLING, W. T. 1986 *Numerical Recipes, The Art of Scientific Computing*. Cambridge University Press.

PROVANSAL, M., MATHIS, C. & BOYER, L. 1987 Bénard–von Kármán instability: transient and forced regimes. *J. Fluid Mech.* **182**, 1–22.

ROUSSOPOULOS, K. 1993 Feedback control of vortex shedding at low Reynolds numbers. *J. Fluid Mech.* **248**, 267–296.

SREENIVASAN, K. R., STRYKOWSKI, P. J. & OLINGER, D. J. 1987 Hopf bifurcation, Landau equation, and vortex shedding behind circular cylinders. In *Forum on Unsteady Flow Separation* (ed. K. N. Ghia), p. 1. ASME FED vol. 52.

SREENIVASAN, K. R., STRYKOWSKI, P. J. & OLINGER, D. J. 1991 On the Hopf bifurcation and Landau–Stuart constants associated with vortex 'shedding' behind circular cylinders. Unpublished.

TOMBOULIDES, A. G., TRIANTAFYLLOU, G. S. & KARNIADAKIS, G. E. 1992 A mechanism of period doubling in free shear flows. *Phys. Fluids* A **4**, 1329–1332.

TRIANTAFYLLOU, G. S. 1990 Three-dimensional flow patterns in two-dimensional wakes. In *Intl Symp. on Nonsteady Fluid Dynamics*, p. 395–402. ASME.

WILLIAMSON, C. H. K. 1988*a* Defining a universal and continuous Strouhal–Reynolds number relationship for the laminar vortex shedding of a circular cylinder. *Phys. Fluids* **31**, 2742–2744.

WILLIAMSON, C. H. K. 1988*b* The existence of two stages in the transition to three-dimensionality of a cylinder wake. *Phys. Fluids* **31**, 3165–3167.

WILLIAMSON, C. H. K. 1989 Oblique and parallel modes of vortex shedding in the wake of a circular cylinder at low Reynolds numbers. *J. Fluid Mech.* **206**, 579–627.

ZEBIB, A. 1987 Stability of viscous flow past a circular cylinder. *J. Engng Maths* **21**, 155–165.